

Rapid Bayesian inference for expensive stochastic models

David J. Warne¹, Ruth E. Baker², and Matthew J. Simpson^{*1}

¹School of Mathematical Sciences, Queensland University of Technology,
Brisbane, Queensland 4001, Australia

²Mathematical Institute, University of Oxford, Oxford, OX2 6GG,
United Kingdom

May 6, 2022

Abstract

Almost all fields of science rely upon statistical inference to estimate unknown parameters in theoretical and computational models. While the performance of modern computer hardware continues to grow, the computational requirements for the simulation of models are growing even faster. This is largely due to the increase in model complexity, often including stochastic dynamics, that is necessary to describe and characterize phenomena observed using modern, high resolution, experimental techniques. Such models are rarely analytically tractable, meaning that extremely large numbers of expensive stochastic simulations are required for parameter inference. In such cases, parameter inference can be practically impossible. In this work, we present new computational Bayesian techniques that accelerate inference for expensive stochastic models by using computationally cheap approximations to inform feasible regions in parameter space, and through learning transforms that adjust the biased approximate inferences to closer represent the correct inferences under the expensive stochastic model. Using topical examples from ecology and cell biology, we demonstrate a speed improvement of an order of magnitude without any loss in accuracy.

Keywords: parameter estimation; statistical inference; continuum-limit approximation; Bayesian inference; approximate Bayesian computation; sequential Monte Carlo

1 Introduction

Modern experimental techniques allow us to observe the natural world in unprecedented detail and resolution [16]. Advances in machine learning and artificial intelligence provide many new techniques for pattern recognition and prediction, however, in almost all scientific inquiry there is a need for detailed mathematical models to provide mechanistic

^{*}To whom correspondence should be addressed. E-mail: matthew.simpson@qut.edu.au

insight into the phenomena observed [2, 20]. This is particularly true in the biological and ecological sciences, where detailed stochastic models are routinely applied to develop and validate theory as well as interpret and analyze data [8, 23, 87].

Two distinct computational challenges arise when stochastic models are considered, they are: (i) the *forwards problem*; and (ii) the *inverse problem*, sometimes called the *backwards problem* [86]. While the computational generation of a single sample path, that is the *forwards problem*, may be feasible, hundreds or thousands or more of such sample paths may be required to gain insight into the range of possible model predictions and to conduct parameter sensitivity analysis [34, 49, 55]. The problem is further compounded if the models must be calibrated using experimental data, that is the *inverse problem* of parameter estimation, since millions of sample paths may be necessary.

In many cases, the forwards problem can be sufficiently computationally expensive to render both parameter sensitivity analysis and the inverse problem completely intractable, despite recent advances in computational inference [69]. This has prompted recent interest in the use of mathematical approximations to circumvent the computational burden, both in the context of the forwards and inverse problems. For example, linear approximations are applied to the forwards problem of chemical reaction networks with bimolecular and higher-order reactions [15], and various approximations, including surrogate models [64] and emulators [13], are applied to inverse problems with expensive forwards models, for example, in the study of climate science [36]. Furthermore, a number of developments, such as multilevel Monte Carlo methods [32], have demonstrated that families of approximations can be combined to improve computational performance without sacrificing accuracy.

In recent years, the Bayesian approach to the inverse problem of model calibration and parameter inference has been particularly successful in many fields of science including, astronomy [75], anthropology and archaeology [43, 54], paleontology and evolution [59, 63, 73], epidemiology [53], biology [46, 80, 89], and ecology [26, 71]. For complex stochastic models, parameterized by θ , computing the likelihood of observing data, \mathcal{D} , is almost always impossible [10, 42, 79]. Thus, approximate Bayesian computation (ABC) methods [69] are essential (Section 4). ABC methods replace likelihood evaluation with an approximation based on stochastic simulations of the proposed model, this is captured directly in *ABC rejection sampling* [5, 63, 73] (Section 2); here \mathcal{M} samples are generated from an approximate posterior using stochastic simulations of the forwards problem as a replacement for the likelihood. Unfortunately, ABC rejection sampling can be computationally expensive or even completely prohibitive, especially for high-dimensional parameter spaces, since a very large number of stochastic simulations are required to generate enough samples from the approximate Bayesian posterior distribution [69]. This is further compounded when the forwards problem is computationally expensive.

In contrast, an appropriately chosen approximate model may yield a tractable likelihood that removes the need for ABC methods [9, 83, 85]. This highlights a key advantage of such approximations because no ABC sampling is required. However, approximations can perform poorly in terms of their predictive capability, and inference based on such models will always be biased, with the extent of the bias dependent on the level of accuracy.

We consider ABC-based inference algorithms for the challenging problem of parameter inference for computationally expensive stochastic models when an appropriate approximation is available to inform the search in parameter space. Under our approach, the approximate model need not be quantitatively accurate in terms of the forwards prob-

lem, but must qualitatively respond to changes in parameter values in a similar way to the stochastic model. In particular, we extend the sequential Monte Carlo ABC sampler (SMC-ABC) of Sisson et al. [68] (Section 2) to exploit the approximate model in two ways:

1. to generate an intermediate proposal distribution, that we call a *preconditioner*, to improve ABC acceptance rates for the stochastic model; and
2. to construct a biased ABC posterior, then reduce this bias using a *moment-matching* transform.

We describe both methods and then present relevant examples from ecology and cell biology. Example calculations demonstrate that our methods generate ABC posteriors with a significant reduction in the number of required expensive stochastic simulations, leading to as much as a tenfold computational speedup.

As a case study for this work, we focus on stochastic models that can replicate many spatiotemporal patterns that naturally arise in biological and ecological systems. Stochastic discrete random walk models (Section 4), henceforth called *discrete models*, can accurately characterize the microscale interactions of individual agents, such as animals, plants, micro-organisms, and cells [1, 18, 45, 74, 78, 81]. Mathematical modeling of populations as complex systems of agents can enhance our understanding of real biological and ecological populations with applications in cancer treatment [12], wound healing [14], wildlife conservation [21, 57], and the management of invasive species [17, 74].

The discrete model formulation can replicate many realistic spatiotemporal patterns. For example, Figure 1(A),(B) demonstrates typical microscopy images obtained from *in vitro* cell culture assays using prostate cancer cells (PC-3 line) and breast cancer cells (MBA-MD-231 line). *In vitro* cell culture assays are ubiquitous and important in the study of cell motility, cell proliferation and drug design. Various patterns are observed: PC-3 cells tend to be highly motile, and spread uniformly to invade vacant spaces (Figure 1(A)); in contrast MBA-MD-231 cells tend to be relatively stationary with proliferation events driving the formation of aggregations (Figure 1(B)). These phenomena may be captured using a lattice-based discrete model framework by varying the ratio P_p/P_m where $P_p \in [0, 1]$ and $P_m \in [0, 1]$ are, respectively, the probabilities that an agent attempts to proliferate and attempts to move during a time interval of duration $\tau > 0$. For $P_p/P_m \ll 1$, behavior akin to PC-3 cells is recovered (Figure 1(C)–(F)) [39]. Setting $P_p/P_m \gg 1$, as in Figure 1(H)–(K), leads to clusters of occupied lattice sites that are similar to the aggregates of MBA-MD-231 cells [1, 65].

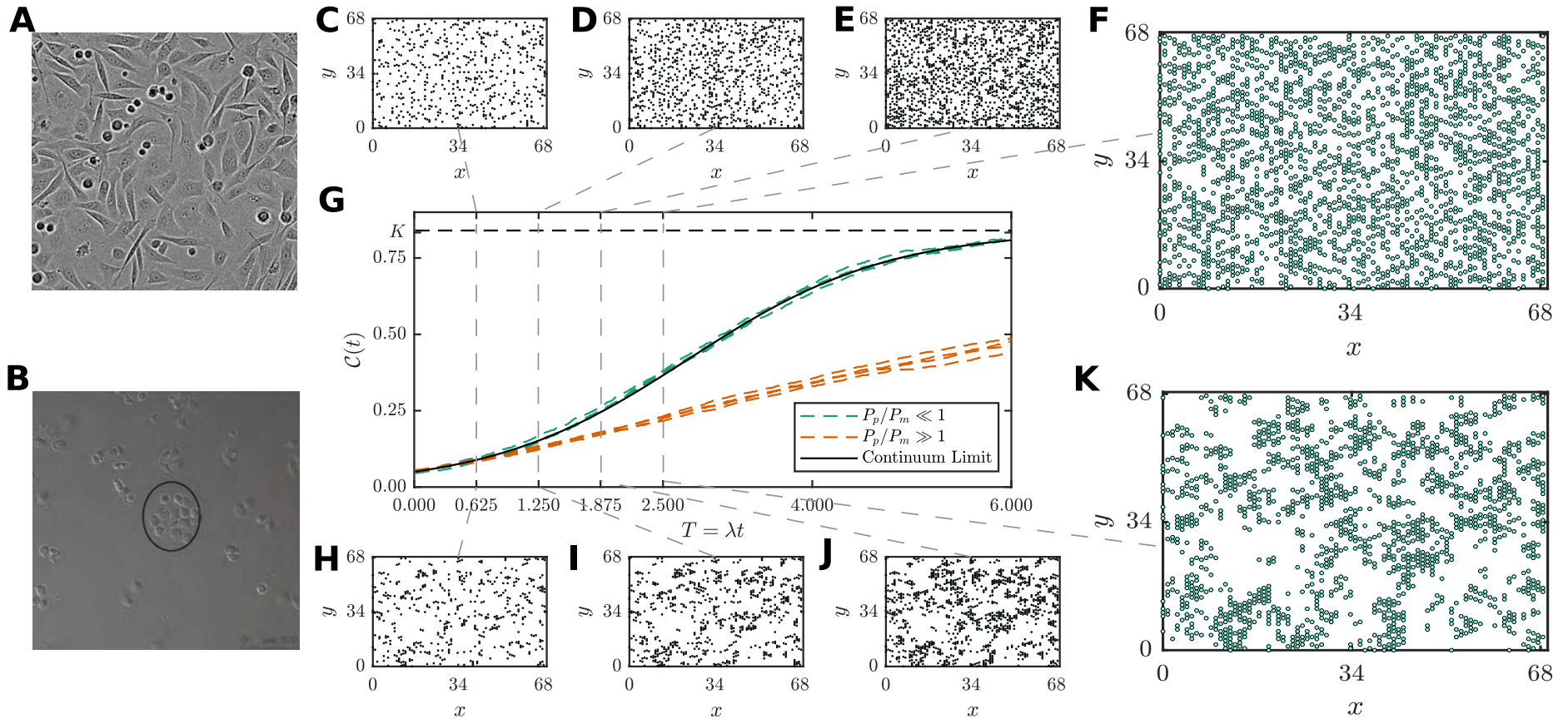


Figure 1: Discrete random walk models can replicate observed spatial patterns in cell culture: (A) PC-3 prostate cancer cells (reprinted from [40] with permission); and (B) MBA-MD-231 breast cancer cells (reprinted from [65] with permission). (C)–(F) Discrete simulations with $P_p/P_m \ll 1$ replicate the uniform distribution of (A) PC-3 cells. (H)–(K) Discrete simulations with $P_p/P_m \gg 1$ replicate spatial clustering of (B) MBA-MD-231 cells. (G) Averaged population density profiles for the discrete model with highly motile agents, $P_m = 1$ (dashed green), and near stationary agents, $P_m = 5 \times 10^{-4}$ (dashed orange), compared with the logistic growth continuum limit (solid black).

It is common practice to derive approximate continuum-limit differential equation descriptions of discrete models [14,39,67] (Section 4). Such approximations provide a means of performing analysis with significantly reduced computational requirements, since evaluating an exact analytical solution, if available, or otherwise numerically solving a differential equation is typically several orders of magnitude cheaper computationally than generating a single realization of the discrete model, of which hundreds or thousands may be required for reliable ABC sampling [10]. However, such approximations are generally only valid within certain parameter regimes, for example here when $P_p/P_m \ll 1$ [14,67]. Consider Figure 1(G), the population density growth curve from the continuum-limit logistic growth model is superimposed with stochastic data for four realizations of a discrete model with $P_p/P_m \ll 1$ and $P_p/P_m \gg 1$, under initial conditions simulating a proliferation assay, where each lattice site is randomly populated with constant probability, such that there are no macroscopic gradients present at $t = 0$. The continuum-limit logistic growth model is an excellent match for the $P_p/P_m \ll 1$ case (Figure 1(C)–(F)), but severely overestimates the population density when $P_p/P_m \gg 1$ since the mean-field assumptions underpinning the continuum-limit model are violated by the presence of clustering (Figure 1(H)–(K)) [1,65].

As we demonstrate in Section 2, our methods generate accurate ABC posteriors for inference on the discrete problem for a range of biologically relevant parameter regimes, including those where the continuum-limit approximation is poor. In this respect we demonstrate a novel use of approximations that qualitatively respond to changes in parameters in a similar way to the full exact stochastic model.

2 Results

In this section, we present details of two new algorithms for the acceleration of ABC inference for expensive stochastic models when an appropriate approximation is available. First, we present essential background in ABC inference and sequential Monte Carlo (SMC) samplers for ABC [68,76]. We then describe our extensions to SMC samplers for ABC and provide numerical examples of our approaches using topical examples from ecology and cell biology.

2.1 Approximate Bayesian computation

Bayesian analysis techniques are powerful tools for the quantification of uncertainty in parameters, models and predictions [31]. Given observations, $\mathcal{D} \in \mathbb{D}$, and a proposed model parameterized by the vector $\boldsymbol{\theta} \in \Theta$, then Bayes’ Theorem states

$$p(\boldsymbol{\theta} \mid \mathcal{D}) = \frac{\mathcal{L}(\boldsymbol{\theta}; \mathcal{D})p(\boldsymbol{\theta})}{\int_{\Theta} \mathcal{L}(\boldsymbol{\theta}; \mathcal{D})p(\boldsymbol{\theta}) \, d\boldsymbol{\theta}},$$

where the *prior*, $p(\boldsymbol{\theta})$, and the *likelihood*, $\mathcal{L}(\boldsymbol{\theta}; \mathcal{D})$, represent assumptions on the parameters and model, respectively. The *posterior*, $p(\boldsymbol{\theta} \mid \mathcal{D})$, quantifies parameter estimates and uncertainty after conditioning on the observations.

Unfortunately, for many stochastic models of practical interest, the likelihood function is intractable. ABC methods replace likelihood evaluation with an approximation based on stochastic simulations of the proposed model, this is captured directly in *ABC rejection sampling* [63,73] (Algorithm 1) where \mathcal{M} samples are generated from an approximate posterior, denoted by $p(\boldsymbol{\theta} \mid \rho(\mathcal{D}, \mathcal{D}_s) \leq \epsilon)$. In Algorithm 1, we have: $\mathcal{D}_s \sim s(\mathcal{D} \mid \boldsymbol{\theta})$

is a data generation process based on simulation of the discrete model; $\rho(\mathcal{D}, \mathcal{D}_s)$ is a discrepancy metric that quantifies the difference between simulations, \mathcal{D}_s , and observations, \mathcal{D} ; and ϵ is the discrepancy threshold. The resulting accepted parameter samples are distributed according to $p(\boldsymbol{\theta} \mid \rho(\mathcal{D}, \mathcal{D}_s) \leq \epsilon) \rightarrow p(\boldsymbol{\theta} \mid \mathcal{D})$ as $\epsilon \rightarrow 0$.

Algorithm 1 ABC rejection sampling

```

1: for  $i = 1, \dots, \mathcal{M}$  do
2:   repeat
3:     Sample prior,  $\boldsymbol{\theta}^* \sim p(\boldsymbol{\theta})$ .
4:     Generate data,  $\mathcal{D}_s \sim s(\mathcal{D} \mid \boldsymbol{\theta}^*)$ .
5:   until  $\rho(\mathcal{D}, \mathcal{D}_s) \leq \epsilon$ 
6:   Set  $\boldsymbol{\theta}^i \leftarrow \boldsymbol{\theta}^*$ .
7: end for

```

By inspection of Algorithm 1, the average acceptance probability of a proposed parameter sample $\boldsymbol{\theta}^*$ is $\mathcal{O}(\epsilon^d)$ [28], where d is the dimensionality of the data space, \mathbb{D} . This renders rejection sampling computationally expensive or even completely prohibitive, especially for high-dimensional parameter spaces [56, 68]. Summary statistics can reduce the data dimensionality, however, they will often incur information loss [4, 28].

2.2 Sequential Monte Carlo for ABC

In the SMC-ABC method, importance resampling is applied to a sequence of R ABC posteriors with discrepancy thresholds $\epsilon_1 > \dots > \epsilon_R$, with ϵ_R indicating the target ABC posterior. Given \mathcal{M} weighted samples $\{(\boldsymbol{\theta}^i, w^i)\}_{i=1}^{\mathcal{M}}$, called particles, from the prior $p(\boldsymbol{\theta})$, particles are filtered through each ABC posterior using three main steps for each particle $\boldsymbol{\theta}^i$:

1. the particle is perturbed using a proposal kernel density $q_r(\boldsymbol{\theta} \mid \boldsymbol{\theta}^i)$;
2. an accept/reject step is performed; and
3. importance weights are updated.

Once all particles have been updated and reweighted, resampling of particles is performed to avoid particle degeneracy. The SMC-ABC algorithm as initially developed by Sisson et al. [68] and Toni et al. [76] is given in Algorithm 2.

Efficient use of SMC-ABC depends critically on the selection of appropriate proposal kernels and threshold sequences. Beaumont et al. [6] and Filippi et al. [30] (Supplementary Material) present methods to determine proposal kernels such that the importance resampling step from ϵ_{r-1} to ϵ_r is efficient, that is, the average acceptance probability is high while still targeting the correct distribution. The efficiency can be evaluated through the Kullback-Leibler divergence [44] of the proposal distribution at ϵ_{r-1} relative to the target distribution at ϵ_r , given by,

$$D_{\text{KL}}(\eta_{r-1}(\cdot); p(\cdot \mid \rho(\mathcal{D}, \mathcal{D}_s) \leq \epsilon_r)) = \int_{\boldsymbol{\Theta}} p(\boldsymbol{\theta}_r \mid \rho(\mathcal{D}, \mathcal{D}_s) \leq \epsilon_r) \log_e \frac{p(\boldsymbol{\theta}_r \mid \rho(\mathcal{D}, \mathcal{D}_s) \leq \epsilon_r)}{\eta_{r-1}(\boldsymbol{\theta}_r)} d\boldsymbol{\theta}_r,$$

where $\eta_{r-1}(\boldsymbol{\theta}_r)$ is the proposal process

$$\eta_{r-1}(\boldsymbol{\theta}_r) = \sum_{j=1}^{\mathcal{M}} q_r(\boldsymbol{\theta}_r \mid \boldsymbol{\theta}_{r-1}^j) w_{r-1}^j. \quad (1)$$

Algorithm 2 SMC-ABC

```

1: Initialize  $\theta_0^i \sim p(\theta)$  and  $w_0^i = \frac{1}{\mathcal{M}}$ , for  $i = 1, \dots, \mathcal{M}$ ;
2: for  $r = 1, \dots, R$  do
3:   for  $i = 1, \dots, \mathcal{M}$  do
4:     repeat
5:       Set  $\theta^* \leftarrow \theta_{r-1}^j$  with probability  $\frac{w_{r-1}^j}{\sum_{k=1}^{\mathcal{M}} w_{r-1}^k}$ ;
6:       Sample transition kernel,  $\theta^{**} \sim q_r(\theta \mid \theta^*)$ ;
7:       Generate data,  $\mathcal{D}_s \sim s(\mathcal{D} \mid \theta^{**})$ ;
8:     until  $\rho(\mathcal{D}, \mathcal{D}_s) \leq \epsilon_r$ 
9:     Set  $\theta_r^i \leftarrow \theta^{**}$ ;
10:    Set  $w_r^i \leftarrow \frac{p(\theta_r^i)}{\sum_{j=1}^{\mathcal{M}} w_{r-1}^j q_r(\theta_r^i \mid \theta_{r-1}^j)}$ ;
11:  end for
12:  Resample weighted particles,  $\{(\theta_r^i, w_r^i)\}_{i=1}^{\mathcal{M}}$ , with replacement;
13:  Set  $w_r^i \leftarrow \frac{1}{\mathcal{M}}$  for all  $i = 1, \dots, \mathcal{M}$ ;
14: end for

```

In an adaptive SMC scheme, the proposal kernel, $q_r(\theta^* \mid \theta)$, is chosen such that the efficiency is optimal under certain assumptions on the kernel and target distribution families (Supplementary Material). In this work, we apply such an adaptive scheme [6, 24, 30] that seeks to select an optimal proposal kernel, $q_r(\theta_r \mid \theta_{r-1})$ based on the weighted samples from the previous iteration $\{(\theta_{r-1}^i, w_{r-1}^i)\}_{i=1}^{\mathcal{M}}$ (Supplementary Material).

2.3 Informing proposals with approximate models

Consider a fixed sequence of ABC posteriors for the stochastic model inference problem, $\{p(\theta \mid \rho(\mathcal{D}, \mathcal{D}_s) \leq \epsilon_r)\}_{r=1}^R$. We want to apply SMC-ABC (Algorithm 2) to efficiently sample from this sequence with adaptive proposal kernels, $\{q_r(\theta^* \mid \theta)\}_{r=1}^R$ [6, 30]. Our method exploits an approximate model to further improve the average acceptance probability.

Say we have a set of weighted particles that represent the ABC posterior at threshold ϵ_{r-1} using the stochastic model, that is, $\{(\theta_{r-1}^i, w_{r-1}^i)\}_{i=1}^{\mathcal{M}} \approx p(\theta_{r-1} \mid \rho(\mathcal{D}, \mathcal{D}_s) \leq \epsilon_{r-1})$. Now, consider applying the next importance resampling step using an approximate data generation step, $\tilde{\mathcal{D}}_s \sim \tilde{s}(\tilde{\mathcal{D}}_s \mid \theta)$, where $\tilde{s}(\tilde{\mathcal{D}}_s \mid \theta)$ is the simulation process of an approximate model¹. The result will be a new set of particles that represent the ABC posterior at threshold ϵ_r using this approximate model, denoted $\{(\tilde{\theta}_r^i, \tilde{w}_r^i)\}_{i=1}^{\mathcal{M}} \approx \tilde{p}(\tilde{\theta}_r \mid \rho(\mathcal{D}, \tilde{\mathcal{D}}_s) \leq \epsilon_r)$. As noted in the examples in Section 1, approximate models are not always valid. This implies that $\tilde{p}(\tilde{\theta}_r \mid \rho(\mathcal{D}, \tilde{\mathcal{D}}_s) \leq \epsilon_r)$ is always biased and will not in general converge to $p(\theta \mid \mathcal{D})$ as $\epsilon_r \rightarrow 0$. However, since the approximation will typically yield a significant computational advantage, it is very cheap to compute the distribution

$$\tilde{\eta}_r(\theta_r) = \sum_{j=1}^{\mathcal{M}} \tilde{q}_r(\theta_r \mid \tilde{\theta}_r^j) \tilde{w}_r^j, \quad (2)$$

¹Throughout, the overbar tilde notation, e.g. \tilde{x} , is used to refer to the ABC entities related to the approximate model.

with proposal kernel $\tilde{q}_r(\boldsymbol{\theta}_r | \tilde{\boldsymbol{\theta}}_r^j)$ that is possibly distinct from the $q_r(\boldsymbol{\theta}_r | \boldsymbol{\theta}_{r-1}^j)$ used in $\eta_{r-1}(\boldsymbol{\theta}_r)$ (Equation (1)). To improve the efficiency of the sampling process we simply require

$$D_{\text{KL}}(\eta_{r-1}(\cdot); p(\cdot | \rho(\mathcal{D}, \mathcal{D}_s) \leq \epsilon_r)) > D_{\text{KL}}(\tilde{\eta}_r(\cdot); p(\cdot | \rho(\mathcal{D}, \tilde{\mathcal{D}}_s) \leq \epsilon_r)), \quad (3)$$

for $\tilde{\eta}_r(\boldsymbol{\theta}_r)$ (Equation (2)) to be more efficient as a proposal mechanism compared with $\eta_{r-1}(\boldsymbol{\theta}_r)$ (Equation (1)). That is, it does not matter that $\tilde{p}(\tilde{\boldsymbol{\theta}}_r | \rho(\mathcal{D}, \tilde{\mathcal{D}}_s) \leq \epsilon_r)$ is biased, it just needs to be less biased than $p(\boldsymbol{\theta}_{r-1} | \rho(\mathcal{D}, \mathcal{D}_s) \leq \epsilon_{r-1})$.

This idea yields an intuitive new algorithm for SMC-ABC; proceed through the sequential sampling of $\{p(\boldsymbol{\theta} | \rho(\mathcal{D}, \mathcal{D}_s) \leq \epsilon_r)\}_{r=1}^R$ by applying two resampling steps for each iteration. The first moves the particles from acceptance threshold ϵ_{r-1} to ϵ_r using the computationally cheap approximate model, and the second corrects for the bias between $\tilde{p}(\tilde{\boldsymbol{\theta}}_r | \rho(\mathcal{D}, \tilde{\mathcal{D}}_s) \leq \epsilon_r)$ and $p(\boldsymbol{\theta}_r | \rho(\mathcal{D}, \mathcal{D}_s) \leq \epsilon_r)$ using the expensive stochastic model, but at an improved acceptance rate. Since the intermediate distribution acts on the proposal

Algorithm 3 Preconditioned SMC-ABC

```

1: Initialize  $\boldsymbol{\theta}_0^i \sim p(\boldsymbol{\theta})$  and  $w_0^i = \frac{1}{\mathcal{M}}$ , for  $i = 1, \dots, \mathcal{M}$ ;
2: for  $r = 1, \dots, R$  do
3:   for  $i = 1, \dots, \mathcal{M}$  do
4:     repeat
5:       Set  $\boldsymbol{\theta}^* \leftarrow \boldsymbol{\theta}_{r-1}^j$  with probability  $\frac{w_{r-1}^j}{\sum_{k=1}^{\mathcal{M}} w_{r-1}^k}$ ;
6:       Sample transition kernel,  $\tilde{\boldsymbol{\theta}}^{**} \sim q_r(\tilde{\boldsymbol{\theta}} | \boldsymbol{\theta}^*)$ ;
7:       Generate data,  $\tilde{\mathcal{D}}_s \sim \tilde{s}(\mathcal{D} | \tilde{\boldsymbol{\theta}}^{**})$ ;
8:       until  $\rho(\mathcal{D}, \tilde{\mathcal{D}}_s) \leq \epsilon_r$ 
9:       Set  $\tilde{\boldsymbol{\theta}}_r^i \leftarrow \tilde{\boldsymbol{\theta}}^{**}$ ;
10:      Set  $\tilde{w}_r^i \leftarrow \frac{p(\tilde{\boldsymbol{\theta}}_r^i)}{\sum_{j=1}^{\mathcal{M}} w_{r-1}^j q_r(\tilde{\boldsymbol{\theta}}_r^i | \boldsymbol{\theta}_{r-1}^j)}$ ;
11:     end for
12:     for  $i = 1, \dots, \mathcal{M}$  do
13:       repeat
14:         Set  $\tilde{\boldsymbol{\theta}}^* \leftarrow \tilde{\boldsymbol{\theta}}_r^j$  with probability  $\frac{\tilde{w}_r^j}{\sum_{k=1}^{\mathcal{M}} \tilde{w}_r^k}$ ;
15:         Sample transition kernel,  $\boldsymbol{\theta}^{**} \sim \tilde{q}_r(\boldsymbol{\theta} | \tilde{\boldsymbol{\theta}}^*)$ ;
16:         Generate data,  $\mathcal{D}_s \sim s(\mathcal{D} | \boldsymbol{\theta}^{**})$ ;
17:         until  $\rho(\mathcal{D}, \mathcal{D}_s) \leq \epsilon_r$ 
18:         Set  $\boldsymbol{\theta}_r^i \leftarrow \boldsymbol{\theta}^{**}$ ;
19:         Set  $w_r^i \leftarrow \frac{p(\boldsymbol{\theta}_r^i)}{\sum_{j=1}^{\mathcal{M}} \tilde{w}_r^j \tilde{q}_r(\boldsymbol{\theta}_r^i | \tilde{\boldsymbol{\theta}}_r^j)}$ ;
20:       end for
21:       Resample weighted particles,  $\{(\boldsymbol{\theta}_r^i, w_r^i)\}_{i=1}^{\mathcal{M}}$ , with replacement;
22:       Set  $w_r^i \leftarrow \frac{1}{\mathcal{M}}$  for all  $i = 1, \dots, \mathcal{M}$ ;
23:     end for

```

mechanism to accelerate the convergence time of SMC-ABC, we denote the sequence

$\{\tilde{p}(\tilde{\boldsymbol{\theta}}_r \mid \rho(\mathcal{D}, \tilde{\mathcal{D}}_s) \leq \epsilon_r)\}_{r=1}^R$ as the preconditioner distribution sequence. The algorithm, called *preconditioned SMC-ABC* (PC-SMC-ABC), is given in Algorithm 3.

One particular advantage of the PC-SMC-ABC method is that it is unbiased, since one could recast PC-SMC-ABC to obtain the SMC-ABC method with a specialized proposal mechanism based on the preconditioner distribution (Supplementary Material). This means that PC-SMC-ABC is completely general, as discussed in Section 3, and is independent of the specific stochastic models that we consider here.

2.4 Using approximations to emulate exact models

The PC-SMC-ABC method is a promising modification to SMC-ABC that can accelerate inference for expensive stochastic models without introducing bias, even for cases where the approximate model is a poor approximation. However, other approaches can be used to obtain further computational improvements. Here, we consider an alternate approach to utilizing approximate models that aims to get the most out of a small sample of expensive stochastic simulations. Unlike PC-SMC-ABC, this method is generally biased, but it has the advantage of yielding a small and fixed computational budget. Specifically, we define a parameter $\alpha \in [0, 1]$, such that $1/\alpha$ is the target computational speedup, for example, $\alpha \approx 1/10$ should result in around 10 times speedup. We apply the SMC-ABC method using $\mathcal{M} = \lfloor (1 - \alpha)\mathcal{M} \rfloor$ particles based on the approximate model, and then use $\hat{\mathcal{M}} = \lceil \alpha\mathcal{M} \rceil$ particles based on the stochastic model to construct a hybrid population of $\mathcal{M} = \hat{\mathcal{M}} + \tilde{\mathcal{M}}$ particles that will represent the final inference on the stochastic model. The key idea is that we use the $\hat{\mathcal{M}}$ particles of the expensive stochastic model to inform a transformation on the $\tilde{\mathcal{M}}$ particles of the approximation such that they emulate particles of expensive stochastic model. Here, $\lfloor \cdot \rfloor$ and $\lceil \cdot \rceil$ are, respectively, the floor and ceiling functions.

Assume that we have applied SMC-ABC to sequentially sample $\tilde{\mathcal{M}}$ particles through the ABC posteriors from the approximate model, $\{\tilde{p}(\tilde{\boldsymbol{\theta}}_r \mid \rho(\mathcal{D}, \tilde{\mathcal{D}}_s) \leq \epsilon_r)\}_{r=1}^R$, with $\epsilon_R = \epsilon$. For the sake of the derivation, say that for all $r \in [1, R]$ we have available the mean vector, $\boldsymbol{\mu}_r$, and the covariance matrix, $\boldsymbol{\Sigma}_r$, of the ABC posterior $p(\boldsymbol{\theta}_r \mid \rho(\mathcal{D}, \mathcal{D}_s) \leq \epsilon_r)$ under the stochastic model. In this case, we use particles $\tilde{\boldsymbol{\theta}}_r^1, \dots, \tilde{\boldsymbol{\theta}}_r^{\tilde{\mathcal{M}}} \sim \tilde{p}(\tilde{\boldsymbol{\theta}}_r \mid \rho(\mathcal{D}, \tilde{\mathcal{D}}_s) \leq \epsilon_r)$ to emulate particles $\boldsymbol{\theta}_r^1, \dots, \boldsymbol{\theta}_r^{\hat{\mathcal{M}}} \sim p(\boldsymbol{\theta}_r \mid \rho(\mathcal{D}, \mathcal{D}_s) \leq \epsilon_r)$ by using the moment matching transform [47, 72]

$$\boldsymbol{\theta}_r^i = \mathbf{L}_r \left[\tilde{\mathbf{L}}_r^{-1} \left(\tilde{\boldsymbol{\theta}}_r^i - \tilde{\boldsymbol{\mu}}_r \right) \right] + \boldsymbol{\mu}_r, \quad i = 1, 2, \dots, \tilde{\mathcal{M}}, \quad (4)$$

where $\tilde{\boldsymbol{\mu}}_r$ and $\tilde{\boldsymbol{\Sigma}}_r$ are the empirical mean vector and covariance matrix of particles $\tilde{\boldsymbol{\theta}}_r^1, \dots, \tilde{\boldsymbol{\theta}}_r^{\tilde{\mathcal{M}}}$, \mathbf{L}_r and $\tilde{\mathbf{L}}_r$ are lower triangular matrices obtained through the Cholesky factorization [62] of $\boldsymbol{\Sigma}_r$ and $\tilde{\boldsymbol{\Sigma}}_r$, respectively, and $\tilde{\mathbf{L}}_r^{-1}$ is the matrix inverse of $\tilde{\mathbf{L}}_r$. This transform will produce a collection of particles that has a sample mean vector of $\boldsymbol{\mu}_r$ and covariance matrix $\boldsymbol{\Sigma}_r$. That is, the transformed sample matches the ABC posterior under the stochastic model up to the first two moments.

In practice, it would be rare that $\boldsymbol{\mu}_r$ and $\boldsymbol{\Sigma}_r$ are known. If $p(\boldsymbol{\theta}_{r-1} \mid \rho(\mathcal{D}, \mathcal{D}_s) \leq \epsilon_{r-1})$ is available, then we can use importance resampling to obtain $\hat{\mathcal{M}}$ particles, $\boldsymbol{\theta}_r^1, \dots, \boldsymbol{\theta}_r^{\hat{\mathcal{M}}}$, from $p(\boldsymbol{\theta}_r \mid \rho(\mathcal{D}, \mathcal{D}_s) \leq \epsilon_r)$, that is, we perform a step from SMC-ABC using the expensive

stochastic model. We can then use the unbiased estimators

$$\hat{\boldsymbol{\mu}}_r = \frac{1}{\hat{\mathcal{M}}} \sum_{i=1}^{\hat{\mathcal{M}}} \boldsymbol{\theta}_r^i \quad \text{and} \quad \hat{\boldsymbol{\Sigma}}_r = \frac{1}{\hat{\mathcal{M}} - 1} \sum_{i=1}^{\hat{\mathcal{M}}} (\boldsymbol{\theta}_r^i - \hat{\boldsymbol{\mu}}_r)(\boldsymbol{\theta}_r^i - \hat{\boldsymbol{\mu}}_r)^\top, \quad (5)$$

to obtain estimates of $\boldsymbol{\mu}_r$ and $\boldsymbol{\Sigma}_r$. Substituting Equation (5) into Equation (4) gives an approximate transform

$$\hat{\boldsymbol{\theta}}_r^i = \hat{\mathbf{L}}_r \left[\tilde{\mathbf{L}}_r^{-1} \left(\tilde{\boldsymbol{\theta}}_r^i - \tilde{\boldsymbol{\mu}}_r \right) \right] + \hat{\boldsymbol{\mu}}_r, \quad i = 1, 2, \dots, \tilde{\mathcal{M}}, \quad (6)$$

where $\hat{\boldsymbol{\Sigma}}_r = \hat{\mathbf{L}}_r \hat{\mathbf{L}}_r^\top$. This enables us to construct an estimate of $p(\boldsymbol{\theta}_r \mid \rho(\mathcal{D}, \mathcal{D}_s) \leq \epsilon_r)$ by applying the moment-matching transform (Equation (6)) to the particles $\tilde{\boldsymbol{\theta}}_r^1, \dots, \tilde{\boldsymbol{\theta}}_r^{\tilde{\mathcal{M}}}$ then pooling the transformed particles $\hat{\boldsymbol{\theta}}_r^1, \dots, \hat{\boldsymbol{\theta}}_r^{\tilde{\mathcal{M}}}$ with the particles $\boldsymbol{\theta}_r^1, \dots, \boldsymbol{\theta}_r^{\hat{\mathcal{M}}}$ that were used in the estimates $\hat{\boldsymbol{\mu}}_r$ and $\hat{\boldsymbol{\Sigma}}_r$. This results in an approximation of $p(\boldsymbol{\theta}_r \mid \rho(\mathcal{D}, \mathcal{D}_s) \leq \epsilon_r)$ using a set of \mathcal{M} particles $\boldsymbol{\theta}_r^1, \dots, \boldsymbol{\theta}_r^{\mathcal{M}}$ with $\boldsymbol{\theta}_r^{i+\hat{\mathcal{M}}} = \hat{\boldsymbol{\theta}}_r^i$ where $1 \leq i \leq \tilde{\mathcal{M}}$.

This leads to our *moment-matching* SMC-ABC (MM-SMC-ABC) method. First, SMC-ABC inference is applied using the approximate model with $\tilde{\mathcal{M}}$ particles. Then, given \mathcal{M} samples from the prior, $p(\boldsymbol{\theta})$, we can sequentially approximate $\{p(\boldsymbol{\theta}_r \mid \rho(\mathcal{D}, \mathcal{D}_s) \leq \epsilon_r)\}_{r=1}^R$. At each iteration the following steps are performed:

1. generate a small number of particles from $p(\boldsymbol{\theta}_r \mid \rho(\mathcal{D}, \mathcal{D}_s) \leq \epsilon_r)$ using importance resampling and stochastic model simulations;
2. compute $\hat{\boldsymbol{\mu}}_r$ and $\hat{\boldsymbol{\Sigma}}_r = \hat{\mathbf{L}}_r \hat{\mathbf{L}}_r^\top$;
3. apply the transform from Equation (6) to the particles at ϵ_r from the approximate model;
4. pool the resulting particles with the stochastic model samples; and
5. reweight particles and resample.

The final MM-SMC-ABC algorithm is provided in Algorithm 4.

The performance of this method depends on the choice of α . Note that in Algorithm 4, standard SMC-ABC for the expensive stochastic model is recovered as $\alpha \rightarrow 1$ (no speedup, inference unbiased), and standard SMC-ABC using the approximate model is recovered as $\alpha \rightarrow 0$ (maximum speedup, but inference biased). Therefore we expect the choice of $0 < \alpha < 1$ to give a trade-off between computational improvement and accuracy. Clearly, the expected speed improvement is proportional to $1/\alpha$, however, if α is chosen to be too small, then the statistical error in the estimates in Equation (5) will be too high. We explore this trade-off in the Supplementary Material and find that $0.05 \leq \alpha \leq 0.2$ seems to give a reasonable result.

Algorithm 4 Moment-matching SMC-ABC

- 1: Given $\alpha \in [0, 1]$, initialize $\hat{\mathcal{M}} = \lceil \alpha \mathcal{M} \rceil$ and $\tilde{\mathcal{M}} = \lfloor (1 - \alpha) \mathcal{M} \rfloor$;
 - 2: Initialize $\tilde{\boldsymbol{\theta}}_0^i \sim p(\boldsymbol{\theta})$ and $\tilde{w}_0^i = \frac{1}{\tilde{\mathcal{M}}}$, for $i = 1, \dots, \tilde{\mathcal{M}}$;
 - 3: Initialize $\boldsymbol{\theta}_0^i \sim p(\boldsymbol{\theta})$ and $w_0^i = \frac{1}{\mathcal{M}}$, for $i = 1, \dots, \mathcal{M}$;
 - 4: Apply SMC-ABC to generate the sequence of approximate particles $\{(\tilde{\boldsymbol{\theta}}_1^i, \tilde{w}_1^i)\}_{i=1}^{\tilde{\mathcal{M}}}$, $\{(\tilde{\boldsymbol{\theta}}_2^i, \tilde{w}_2^i)\}_{i=1}^{\tilde{\mathcal{M}}}, \dots, \{(\tilde{\boldsymbol{\theta}}_R^i, \tilde{w}_R^i)\}_{i=1}^{\tilde{\mathcal{M}}}$;
 - 5: **for** $r = 1, \dots, R$ **do**
 - 6: **for** $i = 1, \dots, \hat{\mathcal{M}}$ **do**
 - 7: **repeat**
 - 8: Set $\boldsymbol{\theta}^* \leftarrow \boldsymbol{\theta}_{r-1}^j$ with probability $\frac{w_r^j}{\sum_{k=1}^{\mathcal{M}} w_{r-1}^k}$;
 - 9: Sample transition kernel, $\boldsymbol{\theta}^{**} \sim q_r(\boldsymbol{\theta} \mid \boldsymbol{\theta}^*)$;
 - 10: Generate data, $\mathcal{D}_s \sim s(\mathcal{D} \mid \boldsymbol{\theta}^{**})$;
 - 11: **until** $\rho(\mathcal{D}, \mathcal{D}_s) \leq \epsilon_r$
 - 12: Set $\boldsymbol{\theta}_r^i \leftarrow \boldsymbol{\theta}^{**}$;
 - 13: Set $w_r^i \leftarrow \frac{p(\boldsymbol{\theta}_r^i)}{\sum_{j=1}^{\mathcal{M}} w_{r-1}^j q_r(\boldsymbol{\theta}_r^i \mid \boldsymbol{\theta}_{r-1}^j)}$;
 - 14: **end for**
 - 15: Estimate means and covariances $\tilde{\boldsymbol{\mu}}_r, \tilde{\boldsymbol{\Sigma}}_r, \hat{\boldsymbol{\mu}}_r$, and $\hat{\boldsymbol{\Sigma}}_r$;
 - 16: Compute Cholesky decompositions $\tilde{\boldsymbol{\Sigma}}_r = \tilde{\mathbf{L}}_r \tilde{\mathbf{L}}_r^\top$ and $\hat{\boldsymbol{\Sigma}}_r = \hat{\mathbf{L}}_r \hat{\mathbf{L}}_r^\top$
 - 17: **for** $i = 1, \dots, \tilde{\mathcal{M}}$ **do**
 - 18: Set $\boldsymbol{\theta}_r^{i+\tilde{\mathcal{M}}} \leftarrow \hat{\mathbf{L}}_r [\tilde{\mathbf{L}}_r^{-1}(\tilde{\boldsymbol{\theta}}_r^i - \tilde{\boldsymbol{\mu}}_r)] + \hat{\boldsymbol{\mu}}_r$ and $w_r^{i+\tilde{\mathcal{M}}} \leftarrow \tilde{w}_r^i$;
 - 19: **end for**
 - 20: Resample weighted particles $\{(\boldsymbol{\theta}_r^i, w_r^i)\}_{i=1}^{\mathcal{M}}$ with replacement;
 - 21: Set $w_r^i \leftarrow 1/\mathcal{M}$ for all $i = 1, \dots, \mathcal{M}$;
 - 22: **end for**
-

2.5 Numerical examples

In this section, we provide numerical examples to demonstrate the accuracy and performance of the PC-SMC-ABC and MM-SMC-ABC methods. For our first example, we consider the analysis of spatially averaged population growth data. The discrete model used in this instance is relevant in the ecological sciences as it describes population growth subject to a weak Allee effect [74]. We then analyze data that is typical of *in vitro* cell culture scratch assays in experimental cell biology using a discrete model that leads to the well-studied Fisher-KPP model [25, 58]. In both examples, we present the discrete model and its continuum limit, then compute the full Bayesian posterior for the model parameters using the PC-SMC-ABC (Algorithm 3) and MM-SMC-ABC (Algorithm 4) methods, and compare the results with the SMC-ABC (Supplementary Material) using either the discrete model or continuum limit alone.

It is important to clarify that when we refer to the accuracy of our methods, we refer to their ability to sample from the target ABC posterior under the expensive stochastic model. The evaluation of this accuracy requires sampling from the target ABC posterior under the expensive stochastic model using SMC-ABC. As a result, the target acceptance thresholds are chosen to ensure this is computationally feasible.

2.5.1 Lattice-based stochastic discrete random walk model

The stochastic discrete model we consider is a lattice-based random walk model that is often used to describe populations of motile cells [39]. The model involves initially placing a population of N agents of size δ on a lattice, L [14,67], for example an $I \times J$ hexagonal lattice [39]. This hexagonal lattice is defined by a set of indices

$L = \{(i, j) : i \in [0, 1, \dots, I - 1], j \in [0, 1, \dots, J - 1]\}$, and a neighborhood function,

$$\mathcal{N}(i, j) = \begin{cases} \{(i - 1, j - 1), (i, j - 1), (i + 1, j - 1), (i + 1, j), (i, j + 1), (i - 1, j)\} & \text{if } i \text{ is even,} \\ \{(i - 1, j), (i, j - 1), (i + 1, j), (i + 1, j + 1), (i, j + 1), (i - 1, j + 1)\} & \text{if } i \text{ is odd.} \end{cases}$$

Lattice indices are mapped to Cartesian coordinates using

$$(x_i, y_j) = \begin{cases} \left(i \frac{\sqrt{3}}{2} \delta, j \delta \right) & \text{if } i \text{ is even,} \\ \left(i \frac{\sqrt{3}}{2} \delta, \left(j + \frac{1}{2} \right) \delta \right) & \text{if } i \text{ is odd.} \end{cases} \quad (7)$$

We define an occupancy function such that $C(\ell, t) = 1$ if site ℓ is occupied by an agent at time $t \geq 0$, otherwise $C(\ell, t) = 0$. This means that in our discrete model each lattice site can be occupied by, at most, one agent.

During each discrete time step of duration τ , agents attempt to move with probability $P_m \in [0, 1]$ and attempt to proliferate with probability $P_p \in [0, 1]$. If an agent at site ℓ attempts a motility event, then a neighboring site will be selected randomly with uniform probability. The motility event is aborted if the selected site is occupied, otherwise the agent will move to the selected site (Figure 2(A)–(C)). For proliferation events, the local neighborhood average occupancy,

$$\hat{C}(\ell, t) = \frac{1}{6} \sum_{\ell' \in \mathcal{N}(\ell)} C(\ell', t),$$

is calculated and a uniform random number $u \sim \mathcal{U}(0, 1)$ is drawn. If $u > f(\hat{C}(\ell, t))$, where $f(\hat{C}(\ell, t)) \in [0, 1]$ is called the *crowding function* [11, 39], then the proliferation event is aborted due to local crowding effects and contact inhibition. If $u \leq f(\hat{C}(\ell, t))$, then proliferation is successful and a daughter agent is placed at a randomly chosen unoccupied lattice site in $\mathcal{N}(\ell)$ (Figure 2(A),(D)–(E)). The evolution of the model is generated through repeating this process through M time steps, $t_1 = \tau, t_2 = 2\tau, \dots, t_M = M\tau$. This approach, based on the work by Jin et al., [39], supports a generic proliferation mechanism since $f(\hat{C}(\ell, t))$ is an arbitrary smooth function passing through $f(0) = 1$ and $f(K) = 0$, where $K > 0$ is the carrying capacity density. However, in the literature there are also examples that include other mechanisms such as cell-cell adhesion [41], directed motility [7], and Allee effects [12].

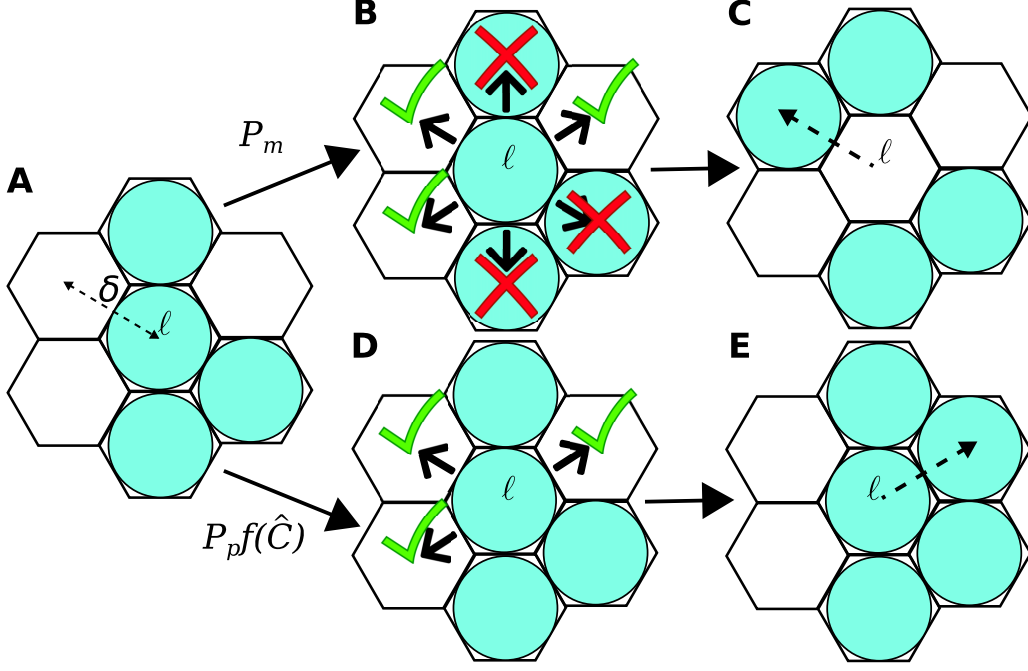


Figure 2: Example of movement and proliferation events in a lattice-based random walk model, using a hexagonal lattice with lattice spacing, δ . (A) An example hexagonal lattice neighborhood $\mathcal{N}(\ell)$. An agent at site ℓ attempts a motility event (A)–(C) with probability P_m . (B) Motility events are aborted when the randomly selected neighbor site is occupied. (C) The agent moves to the selected site, if unoccupied. An agent at site ℓ attempts a proliferation event (A),(D)–(E) with probability P_p . (D) Proliferation events are successful with probability $f(\hat{C}(\ell, t))$, resulting in an unoccupied site being selected. (E) The daughter agent is placed at the selected site and the number of agents in the populations is increased by one.

2.5.2 Approximate continuum-limit descriptions

Discrete models do not generally lend themselves to analytical methods, consequently, their application is intrinsically tied to computationally intensive stochastic simulations and Monte Carlo methods [39]. As a result, it is common practice to approximate mean behavior using differential equations by invoking mean-field assumptions, that is, to treat the occupancy status of lattice sites as independent [14, 67]. The resulting approximate continuum-limit descriptions (Supplementary Material) are partial differential equations (PDEs) of the form

$$\frac{\partial \mathcal{C}(x, y, t)}{\partial t} = D \nabla^2 \mathcal{C}(x, y, t) + \lambda \mathcal{C}(x, y, t) f(\mathcal{C}(x, y, t)), \quad (8)$$

where $\mathcal{C}(x, y, t) = \mathbb{E}[C(\ell, t)]$, $D = \lim_{\delta \rightarrow 0, \tau \rightarrow 0} P_m \delta^2 / (4\tau)$ is the diffusivity, $\lambda = \lim_{\tau \rightarrow 0} P_p / \tau$ is the proliferation rate with $P_p = \mathcal{O}(\tau)$, and $f(\cdot)$ is the crowding function that is related to the proliferation mechanism implemented in the discrete model [11, 39]. For spatially uniform populations there will be no macroscopic spatial gradients on average, that is $\nabla^2 \mathcal{C}(x, y, t) = 0$. Thus, $\mathcal{C}(x, y, t)$ is just a function of time, $\mathcal{C}(t)$, and the continuum limit reduces to an ordinary differential equation (ODE) describing the net population growth,

$$\frac{d\mathcal{C}(t)}{dt} = \lambda \mathcal{C}(t) f(\mathcal{C}(t)). \quad (9)$$

For many standard discrete models, the crowding function is implicitly $f(\mathcal{C}) = 1 - \mathcal{C}$ [14]. That is, the continuum limits in Equation (8) and Equation (9) yield the Fisher-KPP model [25, 58] and the logistic growth model [77, 83], respectively. However, non-logistic growth, for example, $f(\mathcal{C}) = (1 - \mathcal{C})^n$ for $n > 1$, have also been considered [39, 67, 77].

2.5.3 Temporal example: a weak Allee model

The Allee effect refers to the reduction in growth rate of a population at low densities. This is particularly well studied in ecology where there are many mechanisms that give rise to this phenomenon [74]. We introduce an Allee effect into our discrete model by choosing a crowding function of the form

$$f(\hat{C}(\ell, t)) = \left(1 - \frac{\hat{C}(\ell, t)}{K}\right) \left(\frac{A + \hat{C}(\ell, t)}{K}\right),$$

where $\hat{C}(\ell, t) \in [0, 1]$ is the local density at the lattice site $\ell \in L$, at time t , $K > 0$ is the carrying capacity density, and A is the Allee parameter which yields a weak Allee effect for $A \geq 0$ [82]. Note that smaller values of A entail a more pronounced Allee effect with $A < 0$ leading to a strong Allee effect that can lead to species extinction [82]. For simplicity, we only consider the weak Allee effect here, but our methods are general enough to consider any $f(\cdot)$.

Studies in ecology often involve population counts of a particular species over time [74]. In the discrete model, the initial occupancy of each lattice site is independent, leading to no macroscopic spatial gradients on average. It is reasonable to summarize simulations of the discrete model at time t by the average occupancy over the entire lattice, $\bar{C}(t) = (1/IJ) \sum_{\ell \in L} C(\ell, t)$. Therefore, the continuum limit for this case is given by [82]

$$\frac{d\mathcal{C}(t)}{dt} = \lambda \mathcal{C}(t) \left(1 - \frac{\mathcal{C}(t)}{K}\right) \left(\frac{A + \mathcal{C}(t)}{K}\right), \quad (10)$$

with $\mathcal{C}(t) = \mathbb{E}[\bar{C}(t)]$, $\lambda = \lim_{\tau \rightarrow 0} P_p/\tau$, and $\mathcal{C}(0) = \mathbb{E}[\bar{C}(0)]$.

We generate synthetic time-series ecological data using the discrete model, with observations made at times $t_1 = \tau \times 10^3, t_2 = 2\tau \times 10^3, \dots, t_{10} = \tau \times 10^4$, resulting in data $\mathcal{D} = [C_{\text{obs}}(t_1), C_{\text{obs}}(t_2), \dots, C_{\text{obs}}(t_{10})]$ with $C_{\text{obs}}(t) = \bar{C}(t)$ where $\bar{C}(t)$ is the average occupancy at time t for a single realization of the discrete model (Section 4). For this example, we consider an $I \times J$ hexagonal lattice with $I = 80$, $J = 68$, and parameters $P_p = 1/1000$, $P_m = 0$, $\delta = \tau = 1$, $K = 5/6$, and $A = 1/10$. A uniform initial condition is applied, specifically, each site is set to occupied with probability $\mathbb{P}(C(\ell, 0) = 1) = 1/4$ for all $\ell \in L$, giving $\mathcal{C}(0) = 1/4$. This combination of parameters is selected since it is known that the continuum limit (Equation (10)) will not accurately predict the population growth dynamics of the discrete model in this regime (Supplementary Material).

For the inference problem we assume P_m is known, and we seek to compute $p(\boldsymbol{\theta} \mid \mathcal{D})$ under the discrete model with $\boldsymbol{\theta} = [\lambda, A, K]$ and $\lambda = P_p/\tau$. We utilize uninformative priors, $P_p \sim \mathcal{U}(0, 0.005)$, $K \sim \mathcal{U}(0, 1)$ and $A \sim \mathcal{U}(0, 1)$ with the additional constraint that $A \leq K$, that is A and K are not independent in the prior. The discrepancy metric used is the Euclidean distance. For the discrete model, this is

$$\rho(\mathcal{D}, \mathcal{D}_s) = \left[\sum_{j=1}^{10} (C_{\text{obs}}(t_j) - \bar{C}(t_j))^2 \right]^{1/2},$$

where $\bar{C}(t_j)$ is the average occupancy at time t_j of a realization of the discrete model given θ . Similarly, for the continuum limit we have

$$\rho(\mathcal{D}, \tilde{\mathcal{D}}_s) = \left[\sum_{j=1}^{10} (C_{\text{obs}}(t_j) - \mathcal{C}(t_j))^2 \right]^{1/2},$$

where $\mathcal{C}(t_j)$ is the solution to the continuum limit (Equation (10)), computed numerically (Section 4). We compute the posterior using our PC-SMC-ABC and MM-SMC-ABC methods to compare with SMC-ABC under the continuum limit and SMC-ABC under the discrete model. In each instance, $\mathcal{M} = 1000$ particles are used to approach the target threshold $\epsilon = 0.125$ using the sequence $\epsilon_1, \epsilon_2, \dots, \epsilon_5$ with $\epsilon_r = \epsilon_{r-1}/2$. In the case of MM-SMC-ABC the tuning parameter is $\alpha = 0.1$ (Supplementary Material). The Gaussian proposal kernels, $q_r(\theta_r | \theta_{r-1})$ and $\tilde{q}_r(\theta_r | \tilde{\theta}_r)$, are selected adaptively (Supplementary Material).

Figure 3 and Table 1 present the results. SMC-ABC using the continuum-limit model is a poor approximation for SMC-ABC using the discrete model, especially for the proliferation rate parameter, λ (Figure 3(a)), which is expected because $P_m = 0$. However, the posteriors estimated using PC-SMC-ABC are an excellent match to the target posteriors estimated using SMC-ABC with the expensive discrete model, yet the PC-SMC-ABC method requires only half the number of stochastic simulations (Table 1). The MM-SMC-ABC method is not quite as accurate as the PC-SMC-ABC method, however, the number of expensive stochastic simulations is reduced by more than a factor of eight (Table 1) leading to considerable increase in computational efficiency.

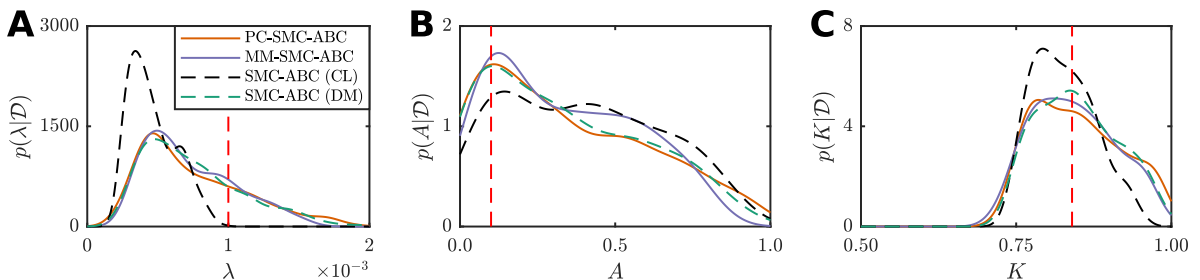


Figure 3: Comparison of estimated posterior marginal densities for the weak Allee model. There is a distinct bias in the SMC-ABC density estimate using the continuum limit (CL) (black dashed) compared with SMC-ABC with the discrete model (DM) (green dashed). However, the density estimates computed using the PC-SMC-ABC (orange solid) and MM-SMC-ABC (purple solid) methods match well with a significantly reduced computational overhead.

Table 1: Computational performance comparison of the SMC-ABC, PC-SMC-ABC, and MM-SMC-ABC methods for the weak Allee model inference problem. Computations are performed using an Intel[®] Xeon[™] E5-2680v3 CPU (2.5 GHz).

Method	Stochastic samples	Continuum samples	Run time (hours)	Speedup
SMC-ABC	28,588	0	47.1	1×
PC-SMC-ABC	13,799	58,752	21.1	2×
MM-SMC-ABC	3,342	36,908	5.6	8×

2.5.4 Spatiotemporal example: a scratch assay

We now look to a discrete model commonly used in studies of cell motility and proliferation, and use spatially extended data that is typical of *in vitro* cell culture experiments, specifically scratch assays [50].

In this case we use a crowding function of the form $f(\hat{C}(\ell, t)) = 1 - \hat{C}(\ell, t)/K$, where $K > 0$ is the carrying capacity density, since it will lead to a logistic growth source term in Equation (8) which characterizes the growth dynamics of many cell types [67, 83]. The discrete model is initialized such that initial density is independent of y . Therefore, we summarize the discrete simulation by computing the average occupancy for each x coordinate, that is, we average over the y -axis in the hexagonal lattice [39], that is, $\bar{C}(x, t) = (1/J) \sum_{(x,y) \in L} C((x, y), t)$. Thus, one arrives at the Fisher-KPP model [25, 58] for the continuum limit,

$$\frac{\partial \mathcal{C}(x, t)}{\partial t} = D \frac{\partial^2 \mathcal{C}(x, t)}{\partial x^2} + \lambda \mathcal{C}(x, t) \left(1 - \frac{\mathcal{C}(x, t)}{K} \right), \quad (11)$$

where $\mathcal{C}(x, t) = \mathbb{E}[\bar{C}(x, t)]$, $D = \lim_{\delta \rightarrow 0, \tau \rightarrow 0} P_m \delta^2 / (4\tau)$, and $\lambda = \lim_{\tau \rightarrow 0} P_p / \tau$.

Just as with the weak Allee model, here we generate synthetic spatiotemporal cell culture data using the discrete model. Observations are made at times $t_1 = 3\tau \times 10^2$, $t_2 = 6\tau \times 10^2, \dots, t_{10} = 3\tau \times 10^3$, resulting in data

$$\mathcal{D} = \begin{bmatrix} C_{\text{obs}}(x_1, t_1) & C_{\text{obs}}(x_1, t_2) & \dots & C_{\text{obs}}(x_1, t_{10}) \\ C_{\text{obs}}(x_2, t_1) & C_{\text{obs}}(x_2, t_2) & \dots & C_{\text{obs}}(x_2, t_{10}) \\ \vdots & \vdots & \ddots & \vdots \\ C_{\text{obs}}(x_I, t_1) & C_{\text{obs}}(x_I, t_2) & \dots & C_{\text{obs}}(x_I, t_{10}) \end{bmatrix},$$

with $C_{\text{obs}}(x, t) = \bar{C}(x, t)$ where $\bar{C}(x, t)$ is the average occupancy over sites $(x, y_1), (x, y_2), \dots, (x, y_J)$ at time t for a single realization of the discrete model. As with the weak Allee model, we consider an $I \times J$ hexagonal lattice with $I = 80$, $J = 68$, and parameters $P_p = 1/1000$, $P_m = 1$, $\delta = \tau = 1$, and $K = 5/6$. We simulate a scratch assay by specifying the center 20 cell columns ($31 \leq i \leq 50$) to be initially unoccupied, and apply a uniform initial condition outside the scratch area such that $\mathbb{E}[C(\ell, 0)] = 1/4$ overall. Note, we have selected a parameter regime for which the continuum limit is an accurate representation of the discrete model average behavior (Supplementary Material).

Since we have spatial information for this problem, we assume P_m is also an unknown parameter and perform inference on the discrete model to compute $p(\boldsymbol{\theta} \mid \mathcal{D})$ with $\boldsymbol{\theta} = [\lambda, D, K]$, $\lambda = P_p / \tau$, and $D = P_m \delta^2 / 4\tau$. We utilize uninformative priors, $P_p \sim \mathcal{U}(0, 0.008)$, $P_m \sim \mathcal{U}(0, 1)$, and $K \sim \mathcal{U}(0, 1)$. For the discrepancy metric we use the Frobenius norm; for the discrete model, this is

$$\rho(\mathcal{D}, \mathcal{D}_s) = \left[\sum_{j=1}^{10} \sum_{i=1}^I (C_{\text{obs}}(x_i, t_j) - \bar{C}(x_i, t_j))^2 \right]^{1/2},$$

where $\bar{C}(x_i, t_j)$ is the average occupancy at site x_i at time t_j of a realization of the discrete model given parameters $\boldsymbol{\theta}$. Similarly, for the continuum limit we have

$$\rho(\mathcal{D}, \tilde{\mathcal{D}}_s) = \left[\sum_{j=1}^{10} \sum_{i=1}^I (C_{\text{obs}}(x_i, t_j) - \mathcal{C}(x_i, t_j))^2 \right]^{1/2},$$

where $\mathcal{C}(x_i, t_j)$ is the solution to the continuum-limit PDE (Equation (11)), computed using a backward-time, centered-space finite difference scheme with fixed-point iteration and adaptive time steps [66, 70] (Section 4). We estimate the posterior using our PC-SMC-ABC and MM-SMC-ABC methods to compare with SMC-ABC using the continuum limit and SMC-ABC using the discrete model. In each case, $\mathcal{M} = 1000$ particles are used to approach the target threshold $\epsilon = 2$ using the sequence $\epsilon_1, \epsilon_2, \dots, \epsilon_5$ with $\epsilon_r = \epsilon_{r-1}/2$. In the case of MM-SMC-ABC the tuning parameter is $\alpha = 0.1$ (Supplementary Material). Again, Gaussian proposal kernels, $q_r(\boldsymbol{\theta}_r | \boldsymbol{\theta}_{r-1})$ and $\tilde{q}_r(\boldsymbol{\theta}_r | \tilde{\boldsymbol{\theta}}_r)$, are selected adaptively (Supplementary Material).

Results are shown in Figure 4 and Table 2. Despite the continuum limit being a good approximation of the discrete model average behavior, using solely this continuum limit in the inference problem still leads to bias. Just as with the weak Allee model, both PC-SMC-ABC and MM-SMC-ABC methods produce a more accurate estimate of the SMC-ABC posterior density with the discrete model. Overall, PC-SMC-ABC is unbiased, however, MM-SMC-ABC is still very accurate. The main point for our work is that the PC-SMC-ABC and MM-SMC-ABC methods both produce posteriors that are accurate compared with the expensive stochastic inference problem, whereas the cheap approximate model alone does not. From Table 2, both PC-SMC-ABC and MM-SMC-ABC require a reduced number of stochastic simulations of the discrete model compared with direct SMC-ABC. For PC-SMC-ABC, the reduction is almost a factor of four, and for MM-SMC-ABC, the reduction is almost a factor of eleven.

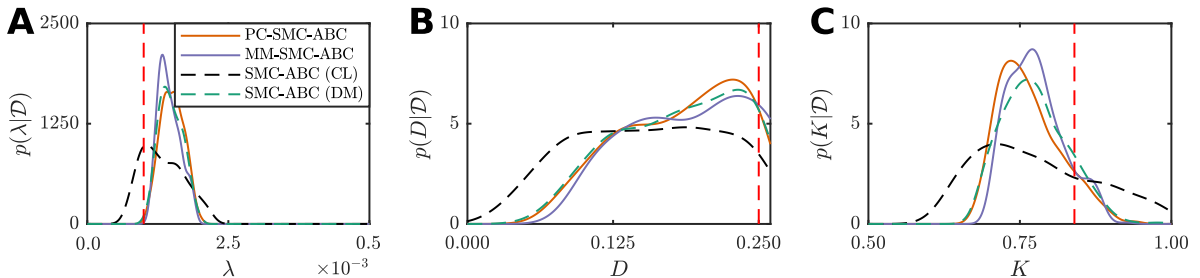


Figure 4: Comparison of estimated posterior marginal densities for the scratch assay model. There is a distinct bias in the SMC-ABC density estimate using the continuum limit (CL) (black dashed) compared with SMC-ABC with the discrete model (DM) (green dashed). However, the density estimates computed using the PC-SMC-ABC (orange solid) and MM-SMC-ABC (purple solid) methods match well with a reduced computational overhead.

Table 2: Computational performance comparison of the SMC-ABC, PC-SMC-ABC, and MM-SMC-ABC methods, using the scratch assay model inference problem. Computations are performed using an Intel[®] Xeon[™] E5-2680v3 CPU (2.5 GHz).

Method	Stochastic samples	Continuum samples	Run time (hours)	Speedup
SMC-ABC	46,435	0	20.6	1×
PC-SMC-ABC	13,949	13,179	5.6	4×
MM-SMC-ABC	4,457	10,594	1.9	11×

2.6 Summary

The two examples presented here demonstrate the efficacy of our two new methods, PC-SMC-ABC and MM-SMC-ABC, for ABC inference with expensive stochastic discrete models. In the first example, the weak Allee model, data were generated using parameters that violate standard continuum-limit assumptions; in the second, the scratch assay model, the Fisher-KPP continuum limit is known to be a good approximation in the parameter regime of the generated data. In both examples, final inferences are biased when the continuum limit is exclusively relied on in the SMC-ABC sampler. However, the results from our new algorithms, PC-SMC-ABC and MM-SMC-ABC, show significantly more accurate posteriors can be computed at a fraction of the cost of the full SMC-ABC using the discrete model, with speed improvements over an order of magnitude.

As mentioned in Section 2.4, the tuning parameter, α , in the MM-SMC-ABC method effectively determines the trade-off between the computational speed of the approximate model and the accuracy of the expensive stochastic model. The values $\alpha = 0$ and $\alpha = 1$ correspond to performing inference exclusively with, respectively, the continuum limit and the stochastic discrete model. Based on numerical experimentation (Supplementary Material), we find that $\alpha \approx 0.1$ is quite reasonable, however, this conclusion will be dependent on the specific model, the parameter space dimensionality, and the number of particles used for the SMC scheme.

3 Discussion

In the life sciences, computationally challenging stochastic discrete models are routinely used to characterize the dynamics of biological populations [14, 18, 67]. In practice, approximations such as the mean-field continuum limit are often derived and used in place of the discrete model for analysis and, more recently, for inference. However, parameter inferences will be biased when the approximate model is solely utilized for inference, even in cases when the approximate model provides an accurate description of the average behavior of the stochastic discrete model.

We provide a new approach to inference for stochastic models that maintains all the methodological benefits of working with discrete mathematical models, while avoiding the computational bottlenecks of relying solely upon repeated expensive stochastic simulations. Our two new algorithms, PC-SMC-ABC and MM-SMC-ABC, utilize samples from the approximate model inference problem in different ways to accelerate SMC-ABC sampling. The PC-SMC-ABC method is unbiased (Supplementary Material), and we demonstrate computational improvements of up to a factor of almost four are possible. If some bias is acceptable, then MM-SMC-ABC can provide further improvements of approximately a factor of ten. In general, the expected speedup will always be around $1/\alpha$, and $\alpha \approx 0.1$ is reasonable based on our numerical investigations (Supplementary Material).

There are some assumptions in our approach that could be generalized in future work. First, in PC-SMC-ABC, we assume that the condition in Equation (3) holds for all ϵ_r ; this is reasonable for the models we consider since we never observe a decrease in performance. However, it may be possible for the bias in the approximate model to be so extreme for some ϵ_r that the condition in Equation (3) is violated, leading to a decrease in performance at specific transitions. Acceptance probabilities could be estimated by performing a small set of trial samples from both $\eta_{r-1}(\boldsymbol{\theta}_{r-1})$ and $\tilde{\eta}_r(\boldsymbol{\theta}_r)$ proposal mecha-

nisms, enabling automatic selection of the optimal proposal mechanism. Second, in the moment matching transform proposed in Equation (4), we use two moments only as this seems to be sufficient for the problems we consider here. However, our methodology is sufficiently flexible that additional moments can be incorporated if necessary.

There are many extensions to our methods that could be considered. We have based our presentation on a form of an SMC-ABC sampler that uses a fixed sequence of thresholds. However, the ideas of using the preconditioning distribution, as in PC-SMC-ABC, and the moment matching transform, as in MM-SMC-ABC, are applicable to SMC schemes that adaptively select thresholds [24]. Recently, there have been a number of state-of-the-art inference schemes introduced based on multilevel Monte Carlo (MLMC) [32,86]. Our new SMC-ABC schemes could exploit MLMC to combine samples from all acceptance thresholds using a coupling scheme and bias correction telescoping summation, such as in the work of Jasra et al. [38] or Warne et al. [84]. Early accept/rejection schemes, such as those considered by Prangle [60], Prescott and Baker [61], and Lester [48], could also be introduced for the sampling steps involving the expensive discrete model.

Delayed acceptance schemes [3,27,33] are also an alternative approach with similar motivations to the methods we propose in this work. However, these approaches can be highly sensitive to false negatives, that is, cases where, for a given θ , the approximate model is rejected but the exact model would have been accepted. Due to this sensitivity to false negatives, the delayed acceptance form of ABC can be biased. Our PC-SMC-ABC approach is not affected by false negatives due to the use of the second set of proposal kernels, $\tilde{q}_r(\theta | \hat{\theta})$. This ensures that PC-SMC-ABC is unbiased, which is a distinct advantage over delayed acceptance ABC.

We have demonstrated our methods using a lattice-based discrete random-walk model that leads to mean-field continuum-limit approximations with linear diffusion and a source term of the form $\lambda \mathcal{C}f(\mathcal{C})$. However, it is important to note that our methods are more widely applicable. We could further generalize the model to deal with a more general class of reaction-diffusion continuum limits involving nonlinear diffusion [85,88] and generalized proliferation mechanisms [65,77]. Our framework is also relevant to lattice-free discrete models [10,18]; we expect the computational improvements will be even more significant in this case. Many other forms of model combinations are also possible. For example, a sequence of continuum models of increasing complexity could be considered, as in Browning et al. [9]. Alternatively, a sequence of numerical approximations of increasing accuracy could be used for inference using a complex target PDE model [19]. Linear mapping approximations of higher order chemical reaction network models, such as in Cao and Grima [15], could also exploit our approach. Another particularly relevant and very general application in systems biology would be to utilize reaction rate equations, that are deterministic ODEs, as approximations to stochastic chemical kinetics models [35,87].

In this work, novel methods have been presented for exploiting approximate models to accelerate Bayesian inference for expensive stochastic models. We have shown that, even when the approximation leads to biased parameter inferences, it can still inform the proposal mechanisms for ABC samplers using the stochastic model. The computational improvements are promising and Bayesian analysis of expensive stochastic models will be more computationally feasible as a result.

4 Methods

This section presents standard computational methods that are applied to *forwards problems* of the models we consider in this work.

4.1 Stochastic simulation of the discrete model

In the work of Jin et al. [39], they consider crowding functions with $f : [0, 1] \rightarrow [0, 1]$. This is not quite sufficient to enable a crowding function with a carrying capacity $K < 1$ since motility events will cause the carrying capacity to be violated. Therefore, we take $f : [0, 1] \rightarrow [-1, 1]$. If $f(\hat{C}(\ell_s)) < 0$ then the site ℓ_s is removed from the set of occupied sites at time t , denoted by $\mathcal{L}(t)$, with probability $P_p |f(\hat{C}(\ell_s))|$. Given these definitions, the lattice-based random walk proceeds according to Algorithm 5.

Algorithm 5 Lattice-based random walk model

```

1: Initialize  $\mathcal{L}(0) \subset L$  with  $|\mathcal{L}(0)| = N$  and  $t \leftarrow 0$ ;
2: while  $t < T$  do
3:    $N \leftarrow |\mathcal{L}(t)|$ ;
4:   for  $i = [1, 2, \dots, N]$  do
5:     Choose  $\ell_s \in \mathcal{L}(t)$  uniformly at random with probability  $\frac{1}{N}$ ;
6:     Choose  $\ell_m \in \mathcal{N}(\ell_s)$  uniformly at random with probability  $\frac{1}{|\mathcal{N}(\ell_s)|}$ ;
7:     if  $C(\ell_m, t) = 0$  then
8:       Generate  $u \sim \mathcal{U}(0, 1)$ ;
9:       if  $u \leq P_m$  then
10:        Set  $\mathcal{L}(t) \leftarrow \{\ell_m\} \cup \mathcal{L}(t) \setminus \{\ell_s\}$ ;
11:       end if
12:     end if
13:   end for
14:   for  $i = [1, 2, \dots, N]$  do
15:     Choose  $\ell_s \in \mathcal{L}(t)$  uniformly at random with probability  $\frac{1}{N}$ ;
16:     Set  $\hat{C}(\ell_s) \leftarrow \frac{1}{|\mathcal{N}(\ell_s)|} \sum_{\ell'_s \in \mathcal{N}(\ell_s)} C(\ell'_s, t)$ ;
17:     Generate  $u \sim \mathcal{U}(0, 1)$ ;
18:     if  $u \leq P_p |f(\hat{C}(\ell_s))|$  then
19:       if  $f(\hat{C}(\ell_s)) \geq 0$  then
20:        Choose  $\ell_p \in \{\ell'_s \in \mathcal{N}(\ell_s) : C(\ell'_s, t) = 0\}$  uniformly at random with probability  $1 - \hat{C}(\ell_s)$ ;
21:        Set  $\mathcal{L}(t) \leftarrow \{\ell_p\} \cup \mathcal{L}(t)$ ;
22:       else
23:        Set  $\mathcal{L}(t) \leftarrow \mathcal{L}(t) \setminus \{\ell_s\}$ ;
24:       end if
25:     end if
26:   end for
27:    $t \leftarrow t + \tau$ 
28: end while

```

4.2 Numerical solutions of continuum-limit differential equations

In our case, the approximate model is a deterministic continuum equation that is either a nonlinear ODE or PDE. In both cases we apply numerical schemes that automatically adapt the time step size to control the truncation error.

4.2.1 ODE numerical solutions

The Runge-Kutta-Fehlberg fourth-order-fifth-order method (RKF45) [29] is a numerical scheme in the Runge-Kutta family of methods to approximate the solution of a nonlinear ODE of the form,

$$\frac{d\mathcal{C}(t)}{dt} = h(t, \mathcal{C}(t)), \quad 0 < t,$$

where $h(t, \mathcal{C}(t))$ is a function that satisfies certain regularity conditions and the initial condition, $\mathcal{C}(0)$.

Given the approximate solution, $c_i \approx \mathcal{C}(t_i)$, an embedded pair of Runge-Kutta methods, specifically a fourth and fifth order pair, are used to advanced the solution to $c_{i+1} \approx \mathcal{C}(t_i + \Delta t) + \mathcal{O}(\Delta t^4)$ and estimate the truncation error that can be used to adaptively adjust Δt to ensure the error is always within some specified tolerance τ .

The fourth and fifth order estimates are, respectively,

$$c_{i+1} = c_i + \Delta t \left(\frac{25}{216}k_1 + \frac{1,408}{2,565}k_3 + \frac{2,197}{4,104}k_4 - \frac{1}{5}k_5 \right), \quad (12)$$

and

$$c_{i+1}^* = c_i + \Delta t \left(\frac{16}{135}k_1 + \frac{6,656}{12,825}k_3 + \frac{28,561}{56,430}k_4 - \frac{9}{50}k_5 + \frac{2}{55}k_6 \right), \quad (13)$$

where

$$\begin{aligned} k_1 &= h(t_i, c_i), \\ k_2 &= h\left(t_i + \frac{\Delta t}{4}, c_i + \frac{\Delta t}{4}k_1\right), \\ k_3 &= h\left(t_i + \frac{3\Delta t}{8}, c_i + \Delta t \left[\frac{3}{32}k_1 + \frac{9}{32}k_2 \right]\right), \\ k_4 &= h\left(t_i + \frac{12\Delta t}{13}, c_i + \Delta t \left[\frac{1,932}{2,197}k_1 - \frac{7,200}{2,197}k_2 + \frac{7,296}{2,197}k_3 \right]\right), \\ k_5 &= h\left(t_i + \Delta t, c_i + \Delta t \left[\frac{439}{216}k_1 - 8k_2 + \frac{3,680}{513}k_3 - \frac{845}{4,104}k_4 \right]\right), \\ k_6 &= h\left(t_i + \frac{\Delta t}{2}, c_i + \Delta t \left[-\frac{8}{27}k_1 + 2k_2 - \frac{3,544}{2,565}k_3 + \frac{1,859}{4,104}k_4 - \frac{11}{40}k_5 \right]\right). \end{aligned}$$

Note that the truncation error can be estimated by $\epsilon = |c_{i+1} - c_{i+1}^*|$. After each evaluation of Equation (12) and Equation (13), a new step size is determined by $\Delta t \leftarrow s\Delta t$, where $s = [\tau/(2\epsilon)]^{1/4}$. If $\epsilon \leq \tau$, then the solution is accepted and the new Δt is used for the next iteration. Alternatively, if $\epsilon > \tau$ then the solution is rejected and a new attempt is made using the new time step. This process is repeated until the solution advances to some desired time point T . For more details and analysis of this method, see Iserles [37].

4.2.2 PDE numerical solutions

In this work, we consider numerical solutions to PDEs of the form

$$\frac{\partial \mathcal{C}(x, t)}{\partial t} = D \frac{\partial^2 \mathcal{C}(x, t)}{\partial x^2} + \lambda \mathcal{C}(x, t) f(\mathcal{C}(x, t)), \quad 0 < t, \quad 0 < x < L, \quad (14)$$

with initial conditions

$$\mathcal{C}(x, 0) = c_0(x), \quad t = 0,$$

and Neumann boundary conditions

$$\frac{\partial \mathcal{C}(x, t)}{\partial x} = 0, \quad x = 0 \text{ and } x = L.$$

Given the approximate solution, $c_i^j \approx \mathcal{C}(x_i, t_j)$ for $i = 1, 2, \dots, N$, then we apply a first order backward Euler discretization in time and first order central differences in space to yield

$$\begin{aligned} \frac{c_2^{j+1} - c_1^{j+1}}{\Delta x} &= 0, \\ \frac{c_i^{j+1} - c_i^j}{\Delta t} &= D \frac{c_{i+1}^{j+1} - 2c_i^{j+1} + c_{i-1}^{j+1}}{\Delta x^2} + \lambda c_i^{j+1} f(c_i^{j+1}), \quad i = 2, 3, \dots, N-1, \\ \frac{c_N^{j+1} - c_{N-1}^{j+1}}{\Delta x} &= 0, \end{aligned} \quad (15)$$

where $c_{i\pm 1}^{j\pm 1} \approx \mathcal{C}(x_i \pm \Delta x, t_j \pm \Delta t)$. The solution is stepped forward in time using fixed point iterations that are initialized by a first order forward Euler estimate.

The truncation error is estimated by

$$\epsilon = \frac{\Delta t}{2} \max_{1 \leq i \leq N} \left| \left(\frac{dc}{dt} \right)_i^{j+1} - \left(\frac{dc}{dt} \right)_i^j \right|, \quad \text{with} \quad \left(\frac{dc}{dt} \right)_i^{j+1} \approx \frac{c_i^{j+1} - c_i^j}{\Delta t}.$$

After solving the nonlinear system (Equation (15)) using fixed point iteration, a new step size is determined by $\Delta t \leftarrow s\Delta t$, where $s = 0.9\sqrt{\tau/\epsilon}$ and τ is the truncation error tolerance [66, 70]. If $\epsilon \leq \tau$, then the solution is accepted and the new Δt is used for the next time step. Alternatively, if $\epsilon > \tau$ then the solution is rejected and a new attempt is made using the new time step. This process is repeated until the solution advances to some desired time point T .

Software availability Numerical examples presented in this work are available from GitHub https://github.com/ProfMJSimpson/Warne_RapidBayesianInference_2019.

Acknowledgements This work was supported by the Australian Research Council (DP170100474). M.J.S. appreciates support from the University of Canterbury Erskine Fellowship. R.E.B. would like to thank the Leverhulme Trust for a Leverhulme Research Fellowship, the Royal Society for a Wolfson Research Merit Award, and the BBSRC for funding via BB/R00816/1.

Computational resources were provided by the eResearch Office, Queensland University of Technology. The authors thank Wang Jin for helpful discussions.

Appendix A Proposal efficiency and adaptive proposal kernels

In the SMC-ABC algorithm, the process of sampling at the target threshold, ϵ_r , given the weights of the previous threshold, ϵ_{r-1} , is described by [30]

$$\xi_r(\boldsymbol{\theta}_r | \mathcal{D}) = \frac{1}{a_{r,r-1}} \int_{\Theta} \int_{\mathbb{D}} \mathbb{1}_{B(\mathcal{D}, \epsilon_r)}(\mathcal{D}_s) s(\mathcal{D}_s | \boldsymbol{\theta}_r) q_r(\boldsymbol{\theta}_r | \boldsymbol{\theta}_{r-1}) w(\boldsymbol{\theta}_{r-1}) d\mathcal{D}_s d\boldsymbol{\theta}_{r-1}, \quad (\text{A.1})$$

where the data space, \mathbb{D} , has dimensionality d , $B(\mathcal{D}, \epsilon_r)$ is a d -dimensional ball centered on the data with radius ϵ_r , and $\mathbb{1}_A(x)$ denotes the indicator function with $\mathbb{1}_A(x) = 1$, if $x \in A$, otherwise $\mathbb{1}_A(x) = 0$. The normalization constant, $a_{r,r-1}$, can be interpreted as the average acceptance probability across all particles. This can be seen by noting that Equation (A.1) can be reduced to

$$\begin{aligned} \xi_r(\boldsymbol{\theta}_r | \mathcal{D}) &= \frac{1}{a_{r,r-1}} \int_{\mathbb{D}} \mathbb{1}_{B(\mathcal{D}, \epsilon_r)}(\mathcal{D}_s) s(\mathcal{D}_s | \boldsymbol{\theta}_r) \left[\int_{\Theta} q_r(\boldsymbol{\theta}_r | \boldsymbol{\theta}_{r-1}) w(\boldsymbol{\theta}_{r-1}) d\boldsymbol{\theta}_{r-1} \right] d\mathcal{D}_s \\ &= \frac{\eta_{r-1}(\boldsymbol{\theta}_r)}{a_{r,r-1}} \int_{\mathbb{D}} \mathbb{1}_{B(\mathcal{D}, \epsilon_r)}(\mathcal{D}_s) s(\mathcal{D}_s | \boldsymbol{\theta}_r) d\mathcal{D}_s \\ &= \frac{\eta_{r-1}(\boldsymbol{\theta}_r) \mathbb{E}[\mathbb{1}_{B(\mathcal{D}, \epsilon_r)}(\mathcal{D}_s) | \boldsymbol{\theta}_r]}{a_{r,r-1}} \\ &= \frac{\eta_{r-1}(\boldsymbol{\theta}_r) \mathbb{P}(\mathcal{D}_s \in B(\mathcal{D}, \epsilon_r) | \boldsymbol{\theta}_r)}{a_{r,r-1}}. \end{aligned} \quad (\text{A.2})$$

Here the distribution $\eta_{r-1}(\boldsymbol{\theta}_r)$ represent the proposal mechanism and $\mathbb{P}(\mathcal{D}_s \in B(\mathcal{D}, \epsilon_r) | \boldsymbol{\theta}_r)$ is the probability that simulated data is within ϵ_r of the data \mathcal{D} given a parameter value $\boldsymbol{\theta}_r$. Therefore, the normalizing constant is

$$\begin{aligned} a_{r,r-1} &= \int_{\Theta} \eta_{r-1}(\boldsymbol{\theta}_r) \mathbb{P}(\mathcal{D}_s \in B(\mathcal{D}, \epsilon_r) | \boldsymbol{\theta}_r) d\boldsymbol{\theta}_r \\ &= \mathbb{E}[\mathbb{P}(\mathcal{D}_s \in B(\mathcal{D}, \epsilon_r) | \boldsymbol{\theta}_r)], \end{aligned} \quad (\text{A.3})$$

that is, $a_{r,r-1}$ is the average acceptance probability.

From a computational perspective, the goal is to choose $\eta_{r-1}(\boldsymbol{\theta}_r)$ to maximize $a_{r,r-1}$. However, this would not necessarily result in a $\xi_r(\boldsymbol{\theta}_r | \mathcal{D})$ that is an accurate approximation to the true target ABC posterior $p(\boldsymbol{\theta}_r | \rho(\mathcal{D}, \mathcal{D}_s) \leq \epsilon_r)$. To achieve this goal, we require $\eta_{r-1}(\boldsymbol{\theta}_r)$ such that the Kullback-Leibler divergence [44], $D_{\text{KL}}(\xi_r(\cdot | \mathcal{D}); p(\cdot | \rho(\mathcal{D}, \mathcal{D}_s) \leq \epsilon_r))$, is minimized.

Beaumont et al. [6] and Filippi et al. [30] demonstrate how the latter goal provides insight into how to optimally choose $\eta_{r-1}(\boldsymbol{\theta}_r)$. The key is to note that $D_{\text{KL}}(\xi_r(\cdot | \mathcal{D}); p(\cdot | \rho(\mathcal{D}, \mathcal{D}_s) \leq \epsilon_r))$ can be decomposed as follows,

$$\begin{aligned} D_{\text{KL}}(\xi_r(\cdot | \mathcal{D}); p(\cdot | \rho(\mathcal{D}, \mathcal{D}_s) \leq \epsilon_r)) &= \int_{\Theta} p(\boldsymbol{\theta}_r | \rho(\mathcal{D}, \mathcal{D}_s) \leq \epsilon_r) \log_e \left[\frac{p(\boldsymbol{\theta}_r | \rho(\mathcal{D}, \mathcal{D}_s) \leq \epsilon_r)}{\xi_r(\boldsymbol{\theta}_r | \mathcal{D})} \right] d\boldsymbol{\theta}_r \\ &= \int_{\Theta} p(\boldsymbol{\theta}_r | \rho(\mathcal{D}, \mathcal{D}_s) \leq \epsilon_r) \log_e \left[\frac{a_{r,r-1} p(\boldsymbol{\theta}_r | \rho(\mathcal{D}, \mathcal{D}_s) \leq \epsilon_r)}{\eta_{r-1}(\boldsymbol{\theta}_r) \int_{\mathbb{D}} \mathbb{1}_{B(\mathcal{D}, \epsilon_r)}(\mathcal{D}_s) s(\mathcal{D}_s | \boldsymbol{\theta}_r) d\mathcal{D}_s} \right] d\boldsymbol{\theta}_r \end{aligned}$$

$$\begin{aligned}
&= \int_{\Theta} p(\boldsymbol{\theta}_r \mid \rho(\mathcal{D}, \mathcal{D}_s) \leq \epsilon_r) \log_e \left[\frac{p(\boldsymbol{\theta}_r \mid \rho(\mathcal{D}, \mathcal{D}_s) \leq \epsilon_r)}{\eta_{r-1}(\boldsymbol{\theta}_r)} \right] d\boldsymbol{\theta}_r \\
&\quad + \int_{\Theta} p(\boldsymbol{\theta}_r \mid \rho(\mathcal{D}, \mathcal{D}_s) \leq \epsilon_r) \log_e [a_{r,r-1}] d\boldsymbol{\theta}_r \\
&\quad - \int_{\Theta} p(\boldsymbol{\theta}_r \mid \rho(\mathcal{D}, \mathcal{D}_s) \leq \epsilon_r) \log_e \left[\int_{\mathbb{D}} \mathbb{1}_{B(\mathcal{D}, \epsilon_r)}(\mathcal{D}_s) s(\mathcal{D}_s \mid \boldsymbol{\theta}_r) d\mathcal{D}_s \right] d\boldsymbol{\theta}_r \\
&= D_{\text{KL}}(\eta_{r-1}(\cdot); p(\cdot \mid \rho(\mathcal{D}, \mathcal{D}_s) \leq \epsilon_r)) - \mathbb{E} \left[\log_e \left(\int_{\mathbb{D}} \mathbb{1}_{B(\mathcal{D}, \epsilon_r)}(\mathcal{D}_s) s(\mathcal{D}_s \mid \boldsymbol{\theta}_r) d\mathcal{D}_s \right) \right] + \log_e a_{r,r-1} \\
&= D_{\text{KL}}(\eta_{r-1}(\cdot); p(\cdot \mid \rho(\mathcal{D}, \mathcal{D}_s) \leq \epsilon_r)) - E(\boldsymbol{\theta}_r) + \log_e a_{r,r-1}, \tag{A.4}
\end{aligned}$$

where $E(\boldsymbol{\theta}_r) = \mathbb{E} \left[\log_e \left(\int_{\mathbb{D}} \mathbb{1}_{B(\mathcal{D}, \epsilon_r)}(\mathcal{D}_s) s(\mathcal{D}_s \mid \boldsymbol{\theta}_r) d\mathcal{D}_s \right) \right]$ is independent of $\eta_{r-1}(\boldsymbol{\theta}_r)$. By rearranging Equation (A.4), we obtain

$$D_{\text{KL}}(\eta_{r-1}(\cdot); p(\cdot \mid \rho(\mathcal{D}, \mathcal{D}_s) \leq \epsilon_r)) = D_{\text{KL}}(\xi_r(\cdot \mid \mathcal{D}); p(\cdot \mid \rho(\mathcal{D}, \mathcal{D}_s) \leq \epsilon_r)) + E(\boldsymbol{\theta}_r) - \log_e a_{r,r-1}.$$

That is, minimizing $D_{\text{KL}}(\eta_{r-1}(\cdot); p(\cdot \mid \rho(\mathcal{D}, \mathcal{D}_s) \leq \epsilon_r))$ is equivalent to minimizing $D_{\text{KL}}(\xi_r(\cdot \mid \mathcal{D}); p(\cdot \mid \rho(\mathcal{D}, \mathcal{D}_s) \leq \epsilon_r))$ and maximizing $a_{r,r-1}$ simultaneously. Therefore, any proposal mechanism that is closer, in the Kullback-Liebler sense, to $p(\cdot \mid \rho(\mathcal{D}, \mathcal{D}_s) \leq \epsilon_r)$ is more efficient.

We apply the optimal adaptive scheme of Beaumont et al. [6] and Filippi et al. [30] for multivariate Gaussian proposals. That is, we set

$$q_r(\boldsymbol{\theta}_r \mid \boldsymbol{\theta}_{r-1}) = \frac{1}{\sqrt{(2\pi)^n \det(\Sigma)}} \exp \left(-(\boldsymbol{\theta}_r - \boldsymbol{\theta}_{r-1})^T \Sigma^{-1} (\boldsymbol{\theta}_r - \boldsymbol{\theta}_{r-1}) / 2 \right),$$

where n is the dimensionality of parameter space, Θ , and

$$\Sigma = \frac{2}{\mathcal{M} - 1} \sum_{i=1}^{\mathcal{M}} (\boldsymbol{\theta}_{r-1}^i - \mu_{r-1})(\boldsymbol{\theta}_{r-1}^i - \mu_{r-1})^T \quad \text{with} \quad \mu_{r-1} = \frac{1}{\mathcal{M}} \sum_{i=1}^{\mathcal{M}} \boldsymbol{\theta}_{r-1}^i.$$

In the PC-SMC-ABC method, we find that independent Gaussian proposals are more effective for the second stage proposal step $\tilde{q}_r(\boldsymbol{\theta}_r^i \mid \tilde{\boldsymbol{\theta}}_r^i)$ since the covariance of the approximate particles $\{\tilde{\boldsymbol{\theta}}_r^i\}_{i=1}^{\mathcal{M}}$ is not a good candidate for the exact target.

Appendix B Analysis of PC-SMC-ABC

Here we demonstrate that the PC-SMC-ABC method is unbiased. In particular, we show that the weighting update scheme can be interpreted as importance sampling on the joint space distribution of particle trajectories and that this joint target density admits the target posterior density as a marginal.

Given the target sequence, $\{p(\boldsymbol{\theta}_r \mid \rho(\mathcal{D}, \mathcal{D}_s) \leq \epsilon_r)\}_{r=1}^R$, and approximate sequence, $\{\tilde{p}(\tilde{\boldsymbol{\theta}}_r \mid \rho(\mathcal{D}, \tilde{\mathcal{D}}_s) \leq \epsilon_r)\}_{r=1}^R$, with prior $p(\boldsymbol{\theta}_0)$, $\epsilon_{r-1} > \epsilon_r$ and proposal kernels $\tilde{q}_r(\boldsymbol{\theta}_r \mid \tilde{\boldsymbol{\theta}}_r)$ and $q_r(\boldsymbol{\theta}_r \mid \boldsymbol{\theta}_{r-1})$, we write the unnormalized weighting update scheme for PC-SMC-ABC. That is,

$$\tilde{w}_r^i = w_{r-1}^i \frac{p(\tilde{\boldsymbol{\theta}}_r^i \mid \rho(\mathcal{D}, \tilde{\mathcal{D}}_s) \leq \epsilon_r) Q_{r-1}(\boldsymbol{\theta}_{r-1}^i \mid \tilde{\boldsymbol{\theta}}_r^i)}{p(\boldsymbol{\theta}_{r-1}^i \mid \rho(\mathcal{D}, \mathcal{D}_s) \leq \epsilon_{r-1}) q_r(\tilde{\boldsymbol{\theta}}_r^i \mid \boldsymbol{\theta}_{r-1}^i)}, \tag{B.1}$$

and

$$w_r^i = \tilde{w}_r^i \frac{p(\boldsymbol{\theta}_r^i | \rho(\mathcal{D}, \mathcal{D}_s) \leq \epsilon_r) \tilde{Q}_r(\tilde{\boldsymbol{\theta}}_r^i | \boldsymbol{\theta}_r^i)}{p(\tilde{\boldsymbol{\theta}}_r^i | \rho(\mathcal{D}, \tilde{\mathcal{D}}_s) \leq \epsilon_r) \tilde{q}_r(\boldsymbol{\theta}_r^i | \tilde{\boldsymbol{\theta}}_r^i)}, \quad (\text{B.2})$$

where $Q_{r-1}(\boldsymbol{\theta}_{r-1}^i | \tilde{\boldsymbol{\theta}}_r^i)$ and $\tilde{Q}_r(\tilde{\boldsymbol{\theta}}_r^i | \boldsymbol{\theta}_r^i)$ are arbitrary backwards kernels. Substitute Equation (B.1) into Equation (B.2) and simplify as follows,

$$\begin{aligned} w_r^i &= w_{r-1}^i \frac{p(\boldsymbol{\theta}_r^i | \rho(\mathcal{D}, \mathcal{D}_s) \leq \epsilon_r) \tilde{Q}_r(\tilde{\boldsymbol{\theta}}_r^i | \boldsymbol{\theta}_r^i)}{p(\tilde{\boldsymbol{\theta}}_r^i | \rho(\mathcal{D}, \tilde{\mathcal{D}}_s) \leq \epsilon_r) \tilde{q}_r(\boldsymbol{\theta}_r^i | \tilde{\boldsymbol{\theta}}_r^i)} \times \frac{p(\tilde{\boldsymbol{\theta}}_r^i | \rho(\mathcal{D}, \tilde{\mathcal{D}}_s) \leq \epsilon_r) Q_{r-1}(\boldsymbol{\theta}_{r-1}^i | \tilde{\boldsymbol{\theta}}_r^i)}{p(\boldsymbol{\theta}_{r-1}^i | \rho(\mathcal{D}, \mathcal{D}_s) \leq \epsilon_{r-1}) q_r(\tilde{\boldsymbol{\theta}}_r^i | \boldsymbol{\theta}_{r-1}^i)} \\ &= w_{r-1}^i \frac{p(\boldsymbol{\theta}_r^i | \rho(\mathcal{D}, \mathcal{D}_s) \leq \epsilon_r) \tilde{Q}_r(\tilde{\boldsymbol{\theta}}_r^i | \boldsymbol{\theta}_r^i) Q_{r-1}(\boldsymbol{\theta}_{r-1}^i | \tilde{\boldsymbol{\theta}}_r^i)}{p(\boldsymbol{\theta}_{r-1}^i | \rho(\mathcal{D}, \mathcal{D}_s) \leq \epsilon_{r-1}) \tilde{q}_r(\boldsymbol{\theta}_r^i | \tilde{\boldsymbol{\theta}}_r^i) q_r(\tilde{\boldsymbol{\theta}}_r^i | \boldsymbol{\theta}_{r-1}^i)} \times \frac{p(\tilde{\boldsymbol{\theta}}_r^i | \rho(\mathcal{D}, \tilde{\mathcal{D}}_s) \leq \epsilon_r)}{p(\tilde{\boldsymbol{\theta}}_r^i | \rho(\mathcal{D}, \tilde{\mathcal{D}}_s) \leq \epsilon_r)} \\ &= w_{r-1}^i \frac{p(\boldsymbol{\theta}_r^i | \rho(\mathcal{D}, \mathcal{D}_s) \leq \epsilon_r) \tilde{Q}_r(\tilde{\boldsymbol{\theta}}_r^i | \boldsymbol{\theta}_r^i) Q_{r-1}(\boldsymbol{\theta}_{r-1}^i | \tilde{\boldsymbol{\theta}}_r^i)}{p(\boldsymbol{\theta}_{r-1}^i | \rho(\mathcal{D}, \mathcal{D}_s) \leq \epsilon_{r-1}) \tilde{q}_r(\boldsymbol{\theta}_r^i | \tilde{\boldsymbol{\theta}}_r^i) q_r(\tilde{\boldsymbol{\theta}}_r^i | \boldsymbol{\theta}_{r-1}^i)} \times 1. \end{aligned} \quad (\text{B.3})$$

Now, recursively expand the weight update sequence (Equation (B.3)) to obtain the final weight for the i th particle,

$$\begin{aligned} w_R^i &= \frac{p(\boldsymbol{\theta}_1^i | \rho(\mathcal{D}, \mathcal{D}_s) \leq \epsilon_1) \tilde{Q}_1(\tilde{\boldsymbol{\theta}}_1^i | \boldsymbol{\theta}_1^i) Q_0(\boldsymbol{\theta}_0^i | \tilde{\boldsymbol{\theta}}_1^i)}{p(\boldsymbol{\theta}_0^i) \tilde{q}_1(\boldsymbol{\theta}_1^i | \tilde{\boldsymbol{\theta}}_1^i) q_1(\tilde{\boldsymbol{\theta}}_1^i | \boldsymbol{\theta}_0^i)} \\ &\quad \times \prod_{r=2}^R \frac{p(\boldsymbol{\theta}_r^i | \rho(\mathcal{D}, \mathcal{D}_s) \leq \epsilon_r) \tilde{Q}_r(\tilde{\boldsymbol{\theta}}_r^i | \boldsymbol{\theta}_r^i) Q_{r-1}(\boldsymbol{\theta}_{r-1}^i | \tilde{\boldsymbol{\theta}}_r^i)}{p(\boldsymbol{\theta}_{r-1}^i | \rho(\mathcal{D}, \mathcal{D}_s) \leq \epsilon_{r-1}) \tilde{q}_r(\boldsymbol{\theta}_r^i | \tilde{\boldsymbol{\theta}}_r^i) q_r(\tilde{\boldsymbol{\theta}}_r^i | \boldsymbol{\theta}_{r-1}^i)} \\ &= \frac{p(\boldsymbol{\theta}_R^i | \rho(\mathcal{D}, \mathcal{D}_s) \leq \epsilon_R)}{p(\boldsymbol{\theta}_0^i)} \prod_{r=1}^R \frac{\tilde{Q}_r(\tilde{\boldsymbol{\theta}}_r^i | \boldsymbol{\theta}_r^i) Q_{r-1}(\boldsymbol{\theta}_{r-1}^i | \tilde{\boldsymbol{\theta}}_r^i)}{\tilde{q}_r(\boldsymbol{\theta}_r^i | \tilde{\boldsymbol{\theta}}_r^i) q_r(\tilde{\boldsymbol{\theta}}_r^i | \boldsymbol{\theta}_{r-1}^i)} \\ &= \frac{p(\boldsymbol{\theta}_R^i | \rho(\mathcal{D}, \mathcal{D}_s) \leq \epsilon_R)}{p(\boldsymbol{\theta}_0^i)} \frac{\prod_{r=1}^R B_{r-1}(\boldsymbol{\theta}_{r-1}^i | \boldsymbol{\theta}_r^i)}{\prod_{r=1}^R F_r(\boldsymbol{\theta}_r^i | \boldsymbol{\theta}_{r-1}^i)}, \end{aligned} \quad (\text{B.4})$$

where $F_r(\boldsymbol{\theta}_r^i | \boldsymbol{\theta}_{r-1}^i) = \tilde{q}_r(\boldsymbol{\theta}_r^i | \tilde{\boldsymbol{\theta}}_r^i) q_r(\tilde{\boldsymbol{\theta}}_r^i | \boldsymbol{\theta}_{r-1}^i)$ is the composite proposal kernel and $B_{r-1}(\boldsymbol{\theta}_{r-1}^i | \boldsymbol{\theta}_r^i) = Q_{r-1}(\boldsymbol{\theta}_{r-1}^i | \tilde{\boldsymbol{\theta}}_r^i) \tilde{Q}_r(\tilde{\boldsymbol{\theta}}_r^i | \boldsymbol{\theta}_r^i)$ is the composite backward kernel. We observe that Equation (B.4) is equivalent to the weight obtained from direct importance sampling on the joint space of the entire particle trajectory [22, 68], that is,

$$w_R^i = \frac{\pi_R(\boldsymbol{\theta}_0^i, \boldsymbol{\theta}_1^i, \dots, \boldsymbol{\theta}_R^i)}{\pi_0(\boldsymbol{\theta}_0^i, \boldsymbol{\theta}_1^i, \dots, \boldsymbol{\theta}_R^i)}.$$

Here, the importance distribution, given by

$$\pi_0(\boldsymbol{\theta}_0^i, \boldsymbol{\theta}_1^i, \dots, \boldsymbol{\theta}_R^i) = p(\boldsymbol{\theta}_0^i) \prod_{r=1}^R F_r(\boldsymbol{\theta}_r^i | \boldsymbol{\theta}_{r-1}^i),$$

is the process of sampling from the prior and performing a sequence of kernel transitions. Finally, we note that the target distribution admits the target ABC posterior as a marginal density, that is,

$$\int_{\mathbb{R}^R} \pi_R(\boldsymbol{\theta}_0^i, \boldsymbol{\theta}_1^i, \dots, \boldsymbol{\theta}_R^i) d\boldsymbol{\theta}_0^i \dots d\boldsymbol{\theta}_{R-1}^i = p(\boldsymbol{\theta}_R^i | \rho(\mathcal{D}, \mathcal{D}_s) \leq \epsilon_R).$$

Therefore, for any function $f(\cdot)$ that satisfies certain regularity conditions,

$$\sum_{i=1}^{\mathcal{M}} f(\boldsymbol{\theta}_R^i) w_R^i \rightarrow \int_{\mathbb{R}} f(\boldsymbol{\theta}_R) p(\boldsymbol{\theta}_R \mid \rho(\mathcal{D}, \mathcal{D}_s) \leq \epsilon_R) d\boldsymbol{\theta}_R = \mathbb{E}[f(\boldsymbol{\theta}_R)],$$

as $\mathcal{M} \rightarrow \infty$, that is, the PC-SMC-ABC method is unbiased.

Appendix C Choice of α in MM-SMC-ABC

The performance of MM-SMC-ABC is dependent on the tuning parameter $\alpha \in [0, 1]$. Since MM-SMC-ABC will only propagate $\lceil \alpha \mathcal{M} \rceil$ particles based on the expensive stochastic model, α can be considered as a target computational cost reduction factor with $1/\alpha$ being the target speed up factor. However, intuitively there will be a limit as to how small one can choose α before the statistical error incurred from the estimates of $\boldsymbol{\mu}_r$ and $\boldsymbol{\Sigma}_r$ is large enough to render the approximate moment matching transform inaccurate. It is non-trivial to analyse MM-SMC-ABC to obtain a theoretical guideline for choosing α , therefore we perform a computational benchmark to obtain a heuristic.

For both inverse problems we consider in Section 2.3 of the main manuscript, the weak Allee model and the scratch assay model, we applied MM-SMC-ABC under identical conditions as in the main manuscript except for the sequence $\{\alpha_k\}_{k=0}^5$ with $\alpha_0 = 0.8$ and $\alpha_k = \alpha_{k-1}/2$ for $k > 0$. For each α_k in the sequence, N independent applications of MM-SMC-ABC was applied. The computational cost for each α_k is denoted by $\text{Cost}(\alpha_k)$ and represents the run time in seconds for an application of MM-SMC-ABC with α_k . We also calculate an error metric,

$$\text{Error}(\alpha_k) = J(\boldsymbol{\Theta}_R, \boldsymbol{\Theta}_R(\alpha_k), P),$$

where $\boldsymbol{\Theta}_R = \{\boldsymbol{\theta}_R^i\}_{i=1}^{\mathcal{M}}$ is a set of particles from an application of SMC-ABC using the expensive stochastic model, and $\boldsymbol{\Theta}_R(\alpha_k) = \left(\{\boldsymbol{\theta}_R^i\}_{i=1}^{\lceil \alpha_k \mathcal{M} \rceil} \cup \{\bar{\boldsymbol{\theta}}_R^i\}_{i=1}^{\lfloor (1-\alpha_k)\mathcal{M} \rfloor} \right)$ is the pooled exact and approximate transformed particles from the j th application of MM-SMC-ABC. For $P \in \mathbb{N}$, the function $J(\cdot, \cdot, P)$ is the P -th order empirical moment-matching distance [51, 52, 90], given by

$$J(\mathbf{X}, \mathbf{Y}, P) = \sum_{m=0}^P \sum_{\mathbf{b} \in S_m} \frac{1}{|S_m|^m} \left(\frac{\hat{\boldsymbol{\mu}}(\mathbf{X})^{\mathbf{b}} - \hat{\boldsymbol{\mu}}(\mathbf{Y})^{\mathbf{b}}}{\hat{\boldsymbol{\mu}}(\mathbf{X})^{\mathbf{b}}} \right)^2,$$

for two sample sets $\mathbf{X} = \{\mathbf{x}_1, \mathbf{x}_2, \dots, \mathbf{x}_{\mathcal{M}}\}$ and $\mathbf{Y} = \{\mathbf{y}_1, \mathbf{y}_2, \dots, \mathbf{y}_{\mathcal{M}}\}$ with $\mathbf{x}_i, \mathbf{y}_i \in \mathbb{R}^n$ for $n \geq 1$, and $S_m = \{\mathbf{b} : \mathbf{b} \in \mathbb{N}^n, \|\mathbf{b}\| = m\}$. For any n -dimensional discrete vector $\mathbf{b} = [b_1, b_2, \dots, b_n]^T \in \mathbb{N}^n$, then $\hat{\boldsymbol{\mu}}(\mathbf{X})^{\mathbf{b}}$ is the \mathbf{b} th empirical raw moment of the sample set \mathbf{X} ,

$$\hat{\boldsymbol{\mu}}(\mathbf{X})^{\mathbf{b}} = \frac{1}{\mathcal{M}} \sum_{i=1}^{\mathcal{M}} \mathbf{x}_i^{\mathbf{b}},$$

where $\mathbf{x}_i^{\mathbf{b}} = x_{i,1}^{b_1} \times x_{i,2}^{b_2} \times \dots \times x_{i,n}^{b_n}$.

We estimated the average $\text{Cost}(\alpha_k)$ and $\text{Error}(\alpha_k)$ for each value of α_k for both the weak Allee effect and the scratch assay inverse problems. Figure C.1 displays the estimates and standard errors given $P = 6$ and $N = 10$, with the value of α_k shown. There

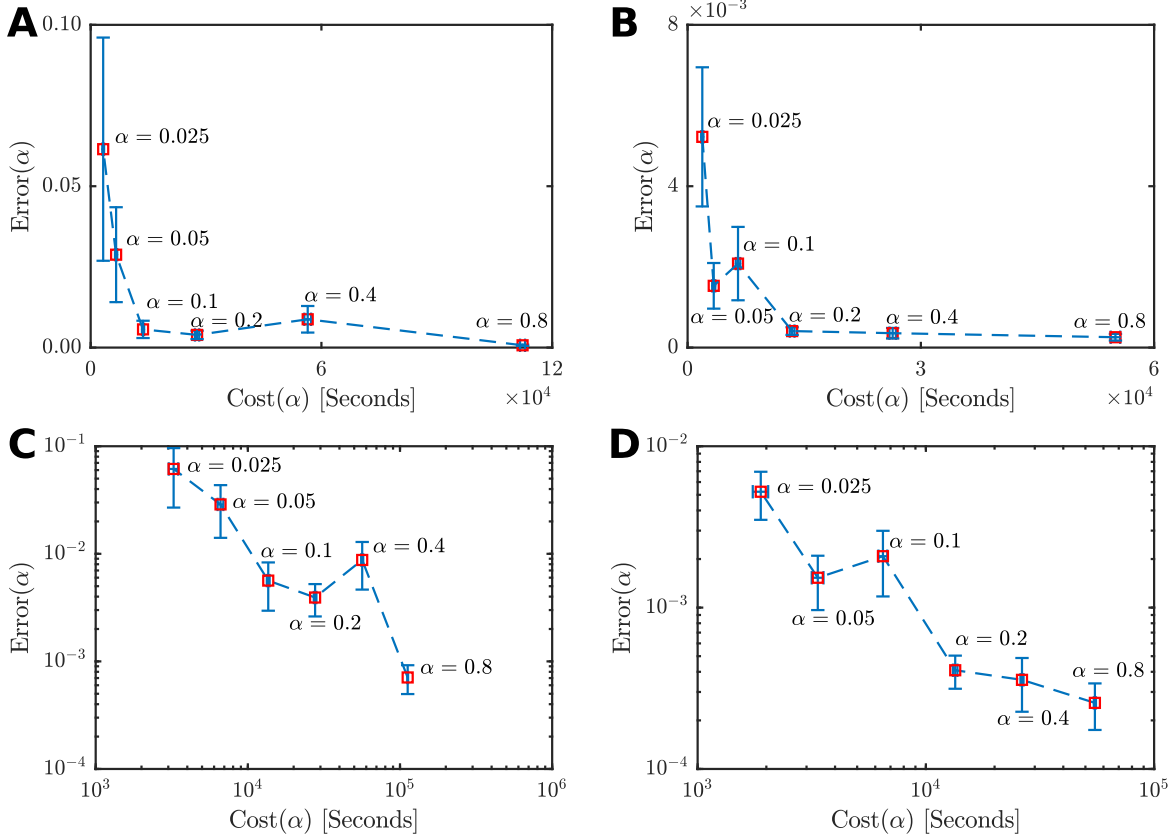


Figure C.1: Cost versus error plots for different values of the tuning parameter α . Averages and standard errors are shown for $N = 10$ independent applications of the MM-SMC-ABC method to the (A) weak Allee effect model (log scale (C)) and (B) the scratch assay model (log scale (D)).

is clearly a threshold for α such that error becomes highly variable if α is smaller than this threshold. For both the weak Allee effect model (Figure C.1(A),(C)) and the scratch assay model (Figure C.1(B),(D)), the optimal choice of α is located between $\alpha_2 = 0.2$ and $\alpha_4 = 0.05$. Therefore, we suggest a heuristic of $\alpha \in [0.1, 0.2]$ to be a reliable choice. If extra performance is needed $\alpha \in [0.05, 0.1]$ may also be acceptable, but if accuracy is of the utmost importance then $\alpha \approx 0.2$ seems to be the most robust choice. In general, the choice of optimal α is still an open problem.

Appendix D Derivation of approximate continuum-limit description

Here we derive the approximate continuum-limit description for our hexagonal lattice based discrete random walk model with generalized crowding function $f : [0, 1] \rightarrow [-1, 1]$. We follow the method of Simpson et al., [67] and Jin et al., [39].

Our main modification is dealing with a potentially negative crowding function. To deal with this case, we define two auxiliary functions,

$$f^+(C) = \begin{cases} f(C) & \text{if } f(C) \geq 0, \\ 0 & \text{otherwise,} \end{cases}, \quad f^-(C) = \begin{cases} |f(C)| & \text{if } f(C) < 0, \\ 0 & \text{otherwise.} \end{cases} \quad (\text{D.1})$$

Note that $f(C) = f^+(C) - f^-(C)$, as this is important later.

We assume a mean-field, that is, for any two lattice sites, $(x_1, y_1), (x_2, y_2) \in \mathbb{R}^2$, then their occupancy probabilities are independent, which results in the property, $\mathbb{E}[C((x_1, y_1), t)C((x_2, y_2), t)] = \mathbb{E}[C((x_1, y_1), t)]\mathbb{E}[C((x_2, y_2), t)]$. Using this property, we denote $\mathcal{C}(x, y, t) = \mathbb{E}[C((x, y), t)]$ and write the conservation of probability equation that describes the change in occupancy probability of a site over a single time step,

$$\begin{aligned} \Delta\mathcal{C}(x, y, t) = & P_m (1 - \mathcal{C}(x, y, t)) \hat{\mathcal{C}}(x, y, t) - P_m \mathcal{C}(x, y, t) (1 - \hat{\mathcal{C}}(x, y, t)) \\ & + \frac{P_p}{6} (1 - \mathcal{C}(x, y, t)) \left(\sum_{(x', y') \in N(x, y)} \mathcal{C}(x', y', t) \frac{f^+(\hat{\mathcal{C}}(x', y', t))}{1 - \hat{\mathcal{C}}(x', y', t)} \right) \\ & - P_p \mathcal{C}(x, y, t) f^-(\hat{\mathcal{C}}(x, y, t)), \end{aligned} \quad (\text{D.2})$$

where $\Delta\mathcal{C}(x, y, t) = \mathcal{C}(x, y, t + \tau) - \mathcal{C}(x, y, t)$,

$$\hat{\mathcal{C}}(x, y, t) = \frac{1}{6} \sum_{(x', y') \in N(x, y)} \mathcal{C}(x', y', t), \quad (\text{D.3})$$

and

$$\hat{\mathcal{C}}(x', y', t) = \frac{1}{6} \sum_{(x'', y'') \in N(x', y')} \mathcal{C}(x'', y'', t). \quad (\text{D.4})$$

The conservation of probability equation (Equation D.2) deserves some interpretation. The first term is the probability that site (x, y) is unoccupied at time t and becomes occupied at time $t + \tau$ due to a successful motility event that moves an agent from an occupied neighboring site into (x, y) . The second term is the probability that site (x, y) is occupied at time t and becomes unoccupied at time $t + \tau$ due to a successful motility event that moves the agent away to a neighboring site. The third term is the probability that site (x, y) is unoccupied at time t and becomes occupied at time $t + \tau$ due to a successful proliferation event from an occupied neighboring site. The final term is the probability that the site (x, y) is occupied at time t and becomes unoccupied at time $t + \tau$ due to $f(\hat{\mathcal{C}}((x, y), t)) < 0$.

For a hexagonal lattice site, (x, y) , we have six immediate neighboring lattice sites, $(x_1, y_1) = (x, y + \delta)$, $(x_2, y_2) = (x, y - \delta)$, $(x_3, y_3) = (x + \delta\sqrt{3}/2, y + \delta/2)$, $(x_4, y_4) = (x - \delta\sqrt{3}/2, y + \delta/2)$, $(x_5, y_5) = (x + \delta\sqrt{3}/2, y - \delta/2)$, and $(x_6, y_6) = (x - \delta\sqrt{3}/2, y - \delta/2)$. The positions of these neighbors are shown in the schematic in Figure D.1. We obtain an expression for $\mathcal{C}(x, y, t)$ at each of the six neighboring lattice points by associating $\mathcal{C}(x, y, t)$ with a continuous function and performing

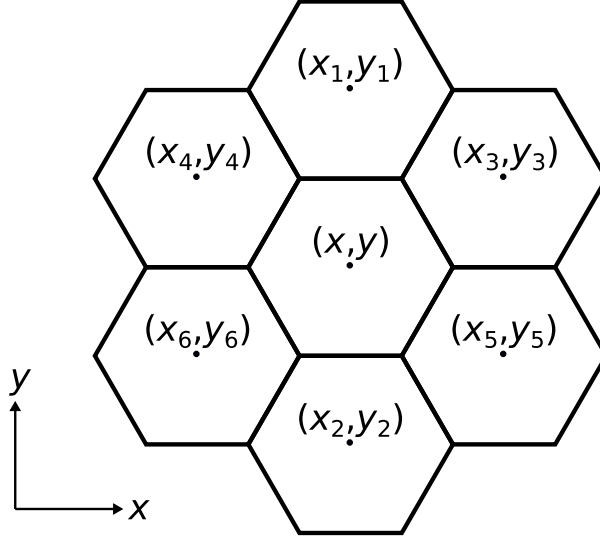


Figure D.1: Schematic of the local neighborhood for the hexagonal lattice. Neighbor coordinates are $(x_1, y_1) = (x, y + \delta)$, $(x_2, y_2) = (x, y - \delta)$, $(x_3, y_3) = (x + \delta\sqrt{3}/2, y + \delta/2)$, $(x_4, y_4) = (x - \delta\sqrt{3}/2, y + \delta/2)$, $(x_5, y_5) = (x + \delta\sqrt{3}/2, y - \delta/2)$, and $(x_6, y_6) = (x - \delta\sqrt{3}/2, y - \delta/2)$.

a Taylor expansion about the point (x, y) . The result is,

$$\begin{aligned}
\mathcal{C}(x_1, y_1, t) &= \mathcal{C}(x, y, t) + \delta \frac{\partial \mathcal{C}(x, y, t)}{\partial y} + \frac{\delta^2}{2} \frac{\partial^2 \mathcal{C}(x, y, t)}{\partial y^2} + \mathcal{O}(\delta^3), \\
\mathcal{C}(x_2, y_2, t) &= \mathcal{C}(x, y, t) - \delta \frac{\partial \mathcal{C}(x, y, t)}{\partial y} + \frac{\delta^2}{2} \frac{\partial^2 \mathcal{C}(x, y, t)}{\partial y^2} + \mathcal{O}(\delta^3), \\
\mathcal{C}(x_3, y_3, t) &= \mathcal{C}(x, y, t) + \frac{\delta\sqrt{3}}{2} \frac{\partial \mathcal{C}(x, y, t)}{\partial x} + \frac{\delta}{2} \frac{\partial \mathcal{C}(x, y, t)}{\partial y} \\
&\quad + \frac{\delta^2}{2} \left[\frac{3}{4} \frac{\partial^2 \mathcal{C}(x, y, t)}{\partial x^2} + \frac{\sqrt{3}}{2} \frac{\partial^2 \mathcal{C}(x, y, t)}{\partial x \partial y} + \frac{1}{4} \frac{\partial^2 \mathcal{C}(x, y, t)}{\partial y^2} \right] + \mathcal{O}(\delta^3), \\
\mathcal{C}(x_4, y_4, t) &= \mathcal{C}(x, y, t) - \frac{\delta\sqrt{3}}{2} \frac{\partial \mathcal{C}(x, y, t)}{\partial x} + \frac{\delta}{2} \frac{\partial \mathcal{C}(x, y, t)}{\partial y} \\
&\quad + \frac{\delta^2}{2} \left[\frac{3}{4} \frac{\partial^2 \mathcal{C}(x, y, t)}{\partial x^2} - \frac{\sqrt{3}}{2} \frac{\partial^2 \mathcal{C}(x, y, t)}{\partial x \partial y} + \frac{1}{4} \frac{\partial^2 \mathcal{C}(x, y, t)}{\partial y^2} \right] + \mathcal{O}(\delta^3), \\
\mathcal{C}(x_5, y_5, t) &= \mathcal{C}(x, y, t) + \frac{\delta\sqrt{3}}{2} \frac{\partial \mathcal{C}(x, y, t)}{\partial x} - \frac{\delta}{2} \frac{\partial \mathcal{C}(x, y, t)}{\partial y} \\
&\quad + \frac{\delta^2}{2} \left[\frac{3}{4} \frac{\partial^2 \mathcal{C}(x, y, t)}{\partial x^2} + \frac{\sqrt{3}}{2} \frac{\partial^2 \mathcal{C}(x, y, t)}{\partial x \partial y} + \frac{1}{4} \frac{\partial^2 \mathcal{C}(x, y, t)}{\partial y^2} \right] + \mathcal{O}(\delta^3), \\
\mathcal{C}(x_6, y_6, t) &= \mathcal{C}(x, y, t) - \frac{\delta\sqrt{3}}{2} \frac{\partial \mathcal{C}(x, y, t)}{\partial x} - \frac{\delta}{2} \frac{\partial \mathcal{C}(x, y, t)}{\partial y} \\
&\quad + \frac{\delta^2}{2} \left[\frac{3}{4} \frac{\partial^2 \mathcal{C}(x, y, t)}{\partial x^2} + \frac{\sqrt{3}}{2} \frac{\partial^2 \mathcal{C}(x, y, t)}{\partial x \partial y} + \frac{1}{4} \frac{\partial^2 \mathcal{C}(x, y, t)}{\partial y^2} \right] + \mathcal{O}(\delta^3).
\end{aligned} \tag{D.5}$$

Therefore, we obtain an expression for $\hat{\mathcal{C}}(x, y, t)$,

$$\begin{aligned}\hat{\mathcal{C}}(x, y, t) &= \frac{1}{6} \sum_{(x', y') \in N(x, y)} \mathcal{C}(x', y', t) \\ &= \frac{1}{6} \sum_{k=1}^6 \mathcal{C}(x_k, y_k, t) \\ &= \mathcal{C}(x, y, t) + \frac{\delta^2}{4} \left[\frac{\partial^2 \mathcal{C}(x, y, t)}{\partial x^2} + \frac{\partial^2 \mathcal{C}(x, y, t)}{\partial y^2} \right] + \mathcal{O}(\delta^3).\end{aligned}\quad (\text{D.6})$$

This expression is required for the first, second, and fourth terms in the conservation equation (Equation (D.2)).

To deal with the third term in Equation (D.2) we require an expression for $g^+(\hat{\mathcal{C}}(x_k, y_k, t)) = f^+(\hat{\mathcal{C}}(x_k, y_k, t))/(1 - \hat{\mathcal{C}}(x_k, y_k, t))$, $k = 1, 2, \dots, 6$. By combining Equation (D.5) and Equation (D.6) we obtain

$$\begin{aligned}\hat{\mathcal{C}}(x_1, y_1, t) &= \mathcal{C}(x, y, t) + \delta \frac{\partial \mathcal{C}(x, y, t)}{\partial y} + \frac{\delta^2}{4} \left[\frac{\partial^2 \mathcal{C}(x, y, t)}{\partial x^2} + 3 \frac{\partial^2 \mathcal{C}(x, y, t)}{\partial y^2} \right] + \mathcal{O}(\delta^3) \\ \hat{\mathcal{C}}(x_2, y_2, t) &= \mathcal{C}(x, y, t) + \delta \frac{\partial \mathcal{C}(x, y, t)}{\partial y} + \frac{\delta^2}{4} \left[\frac{\partial^2 \mathcal{C}(x, y, t)}{\partial x^2} + 3 \frac{\partial^2 \mathcal{C}(x, y, t)}{\partial y^2} \right] + \mathcal{O}(\delta^3) \\ \hat{\mathcal{C}}(x_3, y_3, t) &= \mathcal{C}(x, y, t) + \frac{\delta \sqrt{3}}{2} \frac{\partial \mathcal{C}(x, y, t)}{\partial x} + \frac{\delta}{2} \frac{\partial \mathcal{C}(x, y, t)}{\partial y} \\ &\quad + \frac{\delta^2}{4} \left[\frac{5}{2} \frac{\partial^2 \mathcal{C}(x, y, t)}{\partial x^2} + \sqrt{3} \frac{\partial^2 \mathcal{C}(x, y, t)}{\partial x^2} y + \frac{3}{2} \frac{\partial^2 \mathcal{C}(x, y, t)}{\partial y^2} \right] + \mathcal{O}(\delta^3) \\ \hat{\mathcal{C}}(x_4, y_4, t) &= \mathcal{C}(x, y, t) - \frac{\delta \sqrt{3}}{2} \frac{\partial \mathcal{C}(x, y, t)}{\partial x} + \frac{\delta}{2} \frac{\partial \mathcal{C}(x, y, t)}{\partial y} \\ &\quad + \frac{\delta^2}{4} \left[\frac{5}{2} \frac{\partial^2 \mathcal{C}(x, y, t)}{\partial x^2} - \sqrt{3} \frac{\partial^2 \mathcal{C}(x, y, t)}{\partial x^2} y + \frac{3}{2} \frac{\partial^2 \mathcal{C}(x, y, t)}{\partial y^2} \right] + \mathcal{O}(\delta^3), \\ \hat{\mathcal{C}}(x_5, y_5, t) &= \mathcal{C}(x, y, t) + \frac{\delta \sqrt{3}}{2} \frac{\partial \mathcal{C}(x, y, t)}{\partial x} - \frac{\delta}{2} \frac{\partial \mathcal{C}(x, y, t)}{\partial y} \\ &\quad + \frac{\delta^2}{4} \left[\frac{5}{2} \frac{\partial^2 \mathcal{C}(x, y, t)}{\partial x^2} - \sqrt{3} \frac{\partial^2 \mathcal{C}(x, y, t)}{\partial x^2} y + \frac{3}{2} \frac{\partial^2 \mathcal{C}(x, y, t)}{\partial y^2} \right] + \mathcal{O}(\delta^3), \\ \hat{\mathcal{C}}(x_6, y_6, t) &= \mathcal{C}(x, y, t) - \frac{\delta \sqrt{3}}{2} \frac{\partial \mathcal{C}(x, y, t)}{\partial x} - \frac{\delta}{2} \frac{\partial \mathcal{C}(x, y, t)}{\partial y} \\ &\quad + \frac{\delta^2}{4} \left[\frac{5}{2} \frac{\partial^2 \mathcal{C}(x, y, t)}{\partial x^2} + \sqrt{3} \frac{\partial^2 \mathcal{C}(x, y, t)}{\partial x^2} y + \frac{3}{2} \frac{\partial^2 \mathcal{C}(x, y, t)}{\partial y^2} \right] + \mathcal{O}(\delta^3).\end{aligned}\quad (\text{D.7})$$

Each expression in Equation (D.7) is of the form $\hat{\mathcal{C}}(x_k, y_k, t) = \mathcal{C}(x, y, t) + \bar{\mathcal{C}}_k$, where $\bar{\mathcal{C}}_k = \mathcal{O}(\delta)$. This allows us to consider the Taylor expansion of $g^+(\hat{\mathcal{C}}(x_k, y_k, t))$ about the density $\mathcal{C}(x, y, t)$, that is,

$$g^+(\mathcal{C} + \bar{\mathcal{C}}_k) = g^+(\mathcal{C}) + \bar{\mathcal{C}}_k \frac{dg^+(\mathcal{C})}{d\mathcal{C}} + \frac{\bar{\mathcal{C}}_k^2}{2} \frac{d^2 g^+(\mathcal{C})}{d\mathcal{C}^2} + \mathcal{O}(\delta^3).\quad (\text{D.8})$$

Using Equation (D.8), we can obtain an expression for the summation within the third

term of the conservation equation (Equation (D.2)), that is,

$$\begin{aligned}
\sum_{(x',y') \in N(x,y)} \mathcal{C}(x',y',t) \frac{f^+(\hat{\mathcal{C}}(x',y',t))}{1 - \hat{\mathcal{C}}(x',y',t)} &= \sum_{k=1}^6 \mathcal{C}(x_k, y_k, t) g^+(\mathcal{C}(x, y, t) + \bar{\mathcal{C}}_k) \\
&= g^+(\mathcal{C}(x, y, t)) \sum_{k=1}^6 \mathcal{C}(x_k, y_k, t) + \frac{dg^+(\mathcal{C})}{d\mathcal{C}} \sum_{k=1}^6 \bar{\mathcal{C}}_k \mathcal{C}(x_k, y_k, t) \\
&\quad + \frac{d^2g^+(\mathcal{C})}{d\mathcal{C}^2} \sum_{k=1}^6 \frac{\bar{\mathcal{C}}_k^2}{2} \mathcal{C}(x_k, y_k, t) + \mathcal{O}(\delta^3). \tag{D.9}
\end{aligned}$$

After substitution of Equation (D.7) into Equation (D.9) and some tedious algebra we arrive at

$$\begin{aligned}
\sum_{(x',y') \in N(x,y)} \mathcal{C}(x',y',t) \frac{f^+(\hat{\mathcal{C}}(x',y',t))}{1 - \hat{\mathcal{C}}(x',y',t)} &= 6\mathcal{C}(x, y, t) g^+(\mathcal{C}(x, y, t)) \\
&\quad + \frac{3\delta^2}{2} g^+(\mathcal{C}(x, y, t)) \left[\frac{\partial^2 \mathcal{C}(x, y, t)}{\partial x^2} + \frac{\partial^2 \mathcal{C}(x, y, t)}{\partial y^2} \right] \\
&\quad + 3\delta^2 \mathcal{C}(x, y, t) \frac{dg^+(\mathcal{C})}{d\mathcal{C}} \left[\frac{\partial^2 \mathcal{C}(x, y, t)}{\partial x^2} + \frac{\partial^2 \mathcal{C}(x, y, t)}{\partial y^2} \right] \\
&\quad + 3\delta^2 \frac{dg^+(\mathcal{C})}{d\mathcal{C}} \left[\left(\frac{\partial \mathcal{C}(x, y, t)}{\partial x} \right)^2 + \left(\frac{\partial \mathcal{C}(x, y, t)}{\partial y} \right)^2 \right] \\
&\quad + \frac{3\delta^2}{2} \mathcal{C}(x, y, t) \frac{d^2g^+(\mathcal{C})}{d\mathcal{C}^2} \left[\left(\frac{\partial \mathcal{C}(x, y, t)}{\partial x} \right)^2 + \left(\frac{\partial \mathcal{C}(x, y, t)}{\partial y} \right)^2 \right] \\
&\quad + \mathcal{O}(\delta^3). \tag{D.10}
\end{aligned}$$

Finally, we substitute Equation (D.6) and Equation (D.10) into Equation (D.2) to obtain

$$\begin{aligned}
\Delta \mathcal{C}(x, y, t) &= P_m (1 - \mathcal{C}(x, y, t)) \left[\mathcal{C}(x, y, t) + \frac{\delta^2}{4} \nabla^2 \mathcal{C}(x, y, t) \right] \\
&\quad - P_m \mathcal{C}(x, y, t) \left[1 - \mathcal{C}(x, y, t) - \frac{\delta^2}{4} \nabla^2 \mathcal{C}(x, y, t) \right] \\
&\quad + \frac{P_p}{6} (1 - \mathcal{C}(x, y, t)) \left[6\mathcal{C}(x, y, t) g^+(\mathcal{C}(x, y, t)) + \frac{3\delta^2}{2} g^+(\mathcal{C}(x, y, t)) \nabla^2 \mathcal{C}(x, y, t) \right. \\
&\quad + 3\delta^2 \mathcal{C}(x, y, t) \frac{dg^+(\mathcal{C})}{d\mathcal{C}} \nabla^2 \mathcal{C}(x, y, t) + 3\delta^2 \frac{dg^+(\mathcal{C})}{d\mathcal{C}} (\nabla \mathcal{C}(x, y, t) \cdot \nabla \mathcal{C}(x, y, t)) \\
&\quad \left. + \frac{3\delta^2}{2} \mathcal{C}(x, y, t) \frac{d^2g^+(\mathcal{C})}{d\mathcal{C}^2} (\nabla \mathcal{C}(x, y, t) \cdot \nabla \mathcal{C}(x, y, t)) \right] \\
&\quad - P_p \mathcal{C}(x, y, t) f^-(\mathcal{C}(x, y, t)) + \mathcal{O}(\delta^3). \tag{D.11}
\end{aligned}$$

Here we have used the notation $\nabla^2 \mathcal{C} = \frac{\partial^2 \mathcal{C}}{\partial x^2} + \frac{\partial^2 \mathcal{C}}{\partial y^2}$, and $\nabla \mathcal{C} \cdot \nabla \mathcal{C} = \left(\frac{\partial \mathcal{C}}{\partial x} \right)^2 + \left(\frac{\partial \mathcal{C}}{\partial y} \right)^2$. After rearranging Equation (D.11), we obtain

$$\begin{aligned}
\Delta \mathcal{C}(x, y, t) &= \frac{P_m \delta^2}{4} \nabla^2 \mathcal{C}(x, y, t) + P_p \mathcal{C}(x, y, t) \left[(1 - \mathcal{C}(x, y, t)) g^+(\mathcal{C}(x, y, t)) - f^-(\mathcal{C}(x, y, t)) \right] \\
&\quad + P_p \delta^2 H(\mathcal{C}(x, y, t)) + \mathcal{O}(\delta^3) \tag{D.12}
\end{aligned}$$

where

$$H(\mathcal{C}(x, y, t)) = \frac{1}{4}g^+(\mathcal{C}(x, y, t))\nabla^2\mathcal{C}(x, y, t) + \frac{1}{2}\mathcal{C}(x, y, t)\frac{dg^+(\mathcal{C})}{d\mathcal{C}}\nabla^2\mathcal{C}(x, y, t) \\ + \frac{1}{2}\frac{dg^+(\mathcal{C})}{d\mathcal{C}}(\nabla\mathcal{C}(x, y, t) \cdot \nabla\mathcal{C}(x, y, t)) + \frac{1}{4}\mathcal{C}(x, y, t)\frac{d^2g^+(\mathcal{C})}{d\mathcal{C}^2}(\nabla\mathcal{C}(x, y, t) \cdot \nabla\mathcal{C}(x, y, t)).$$

Note that $f^+(\mathcal{C}(x, y, t)) = g^+(\mathcal{C}(x, y, t))(1 - \mathcal{C}(x, y, t))$ and, by Equation (D.1), that $f(\mathcal{C}(x, y, t)) = f^+(\mathcal{C}(x, y, t)) - f^-(\mathcal{C}(x, y, t))$. Then Equation (D.12) becomes

$$\Delta\mathcal{C}(x, y, t) = \frac{P_m\delta^2}{4}\nabla^2\mathcal{C}(x, y, t) + P_p\mathcal{C}(x, y, t)f(\mathcal{C}(x, y, t)) + P_p\delta^2H(\mathcal{C}(x, y, t)) + \mathcal{O}(\delta^3).$$

After dividing by the time interval, τ , and choosing $\delta^2 = \mathcal{O}(\tau)$ and $P_p = \mathcal{O}(\tau)$, then we have the following limits,

$$\lim_{\tau \rightarrow 0} \frac{P_m\delta^2}{4\tau} = D, \quad \lim_{\tau \rightarrow 0} \frac{P_p}{\tau} = \lambda, \quad \lim_{\tau \rightarrow 0} \frac{\Delta\mathcal{C}(x, y, t)}{\tau} = \frac{\partial\mathcal{C}(x, y, t)}{\partial t}, \quad \lim_{\tau \rightarrow 0} \frac{P_p\delta^2}{\tau} = 0.$$

Therefore, we arrive at the continuum-limit approximation

$$\frac{\partial\mathcal{C}(x, y, t)}{\partial t} = D\nabla^2\mathcal{C}(x, y, t) + \lambda\mathcal{C}(x, y, t)f(\mathcal{C}(x, y, t)).$$

Appendix E Additional results

We provide the multivariate posteriors for the results provided in the main text. In both Figure E.1 and Figure E.2 the contours of the posterior bivariate marginals generated, at a significant reduction in computational cost, both the PC-SMC-ABC and MM-SMC-ABC methods align very well with contours of the posterior bivariate marginals SMC-ABC using the expensive discrete model alone, however, there is a clear bias in the contours posterior bivariate marginals generated with SMC-ABC using the continuum-limit approximation alone.

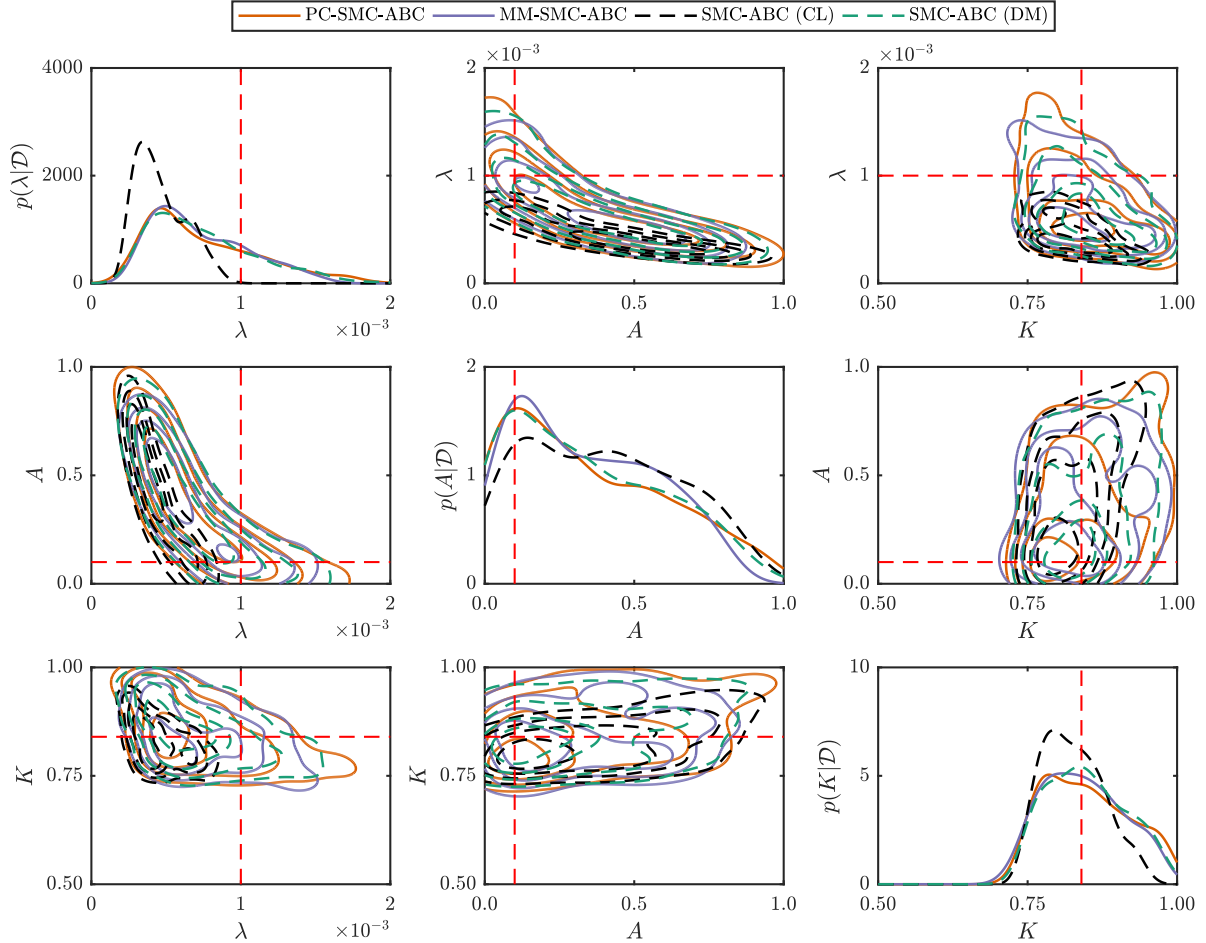


Figure E.1: Comparison of estimated posterior marginal densities for the weak Allee model. There is a distinct bias in the SMC-ABC density estimate using the continuum limit (CL) (black dashed) compared with the SMC-ABC method with the discrete model (DM) (green dashed). However, the density estimates computed using the PC-SMC-ABC (orange solid) and MM-SMC-ABC (purple solid) methods match well with a reduced computational overhead.

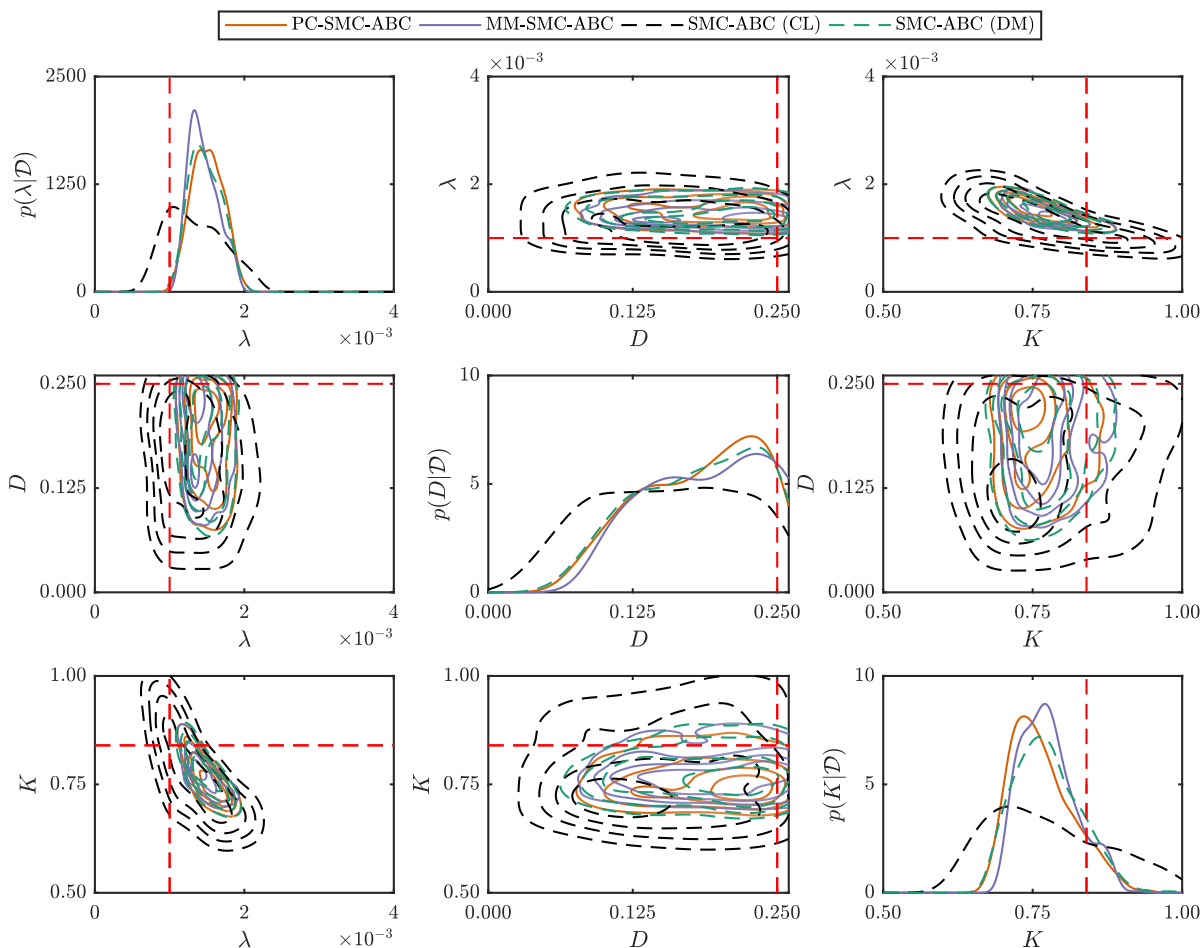


Figure E.2: Comparison of estimated posterior marginal densities for the scratch assay model. There is a distinct bias in the SMC-ABC density estimate using the continuum limit (CL) (black dashed) compared with the SMC-ABC method with the discrete model (DM) (green dashed). However, the density estimates computed using the PC-SMC-ABC (orange solid) and MM-SMC-ABC (purple solid) methods match well with a reduced computational overhead.

Appendix F Effect of motility rate on continuum-limit approximation

Here we demonstrate the ability (or lack thereof) of the continuum-limit approximation to capture the average behavior of the discrete model for the two examples considered in the main manuscript: the weak Allee model; and the scratch assay model. Figure F.1 plots the solutions to the continuum-limit differential equation against realizations of the discrete model for both motile, $P_m = 1$, and non-motile, $P_m = 0$, agents.

In the case of the weak Allee model (Figure F.1(A)), the continuum limit does not match the average behavior in either case, though it does perform better when $P_m = 1$ than when $P_m = 0$. The remaining discrepancy when $P_m = 1$ is can be related to the ratio P_p/P_m and to the effect of the neighborhood radius, r (see Jin et al. [39] for further explanation). Decreasing P_p/P_m and increasing r will correct this discrepancy. The scratch assay continuum limit captures the average behavior of the discrete model very well when $P_m = 1$ (Figure F.1(B)), but does not capture the scratch closing behavior of the discrete model when $P_m = 0$ (Figure F.1(C)).

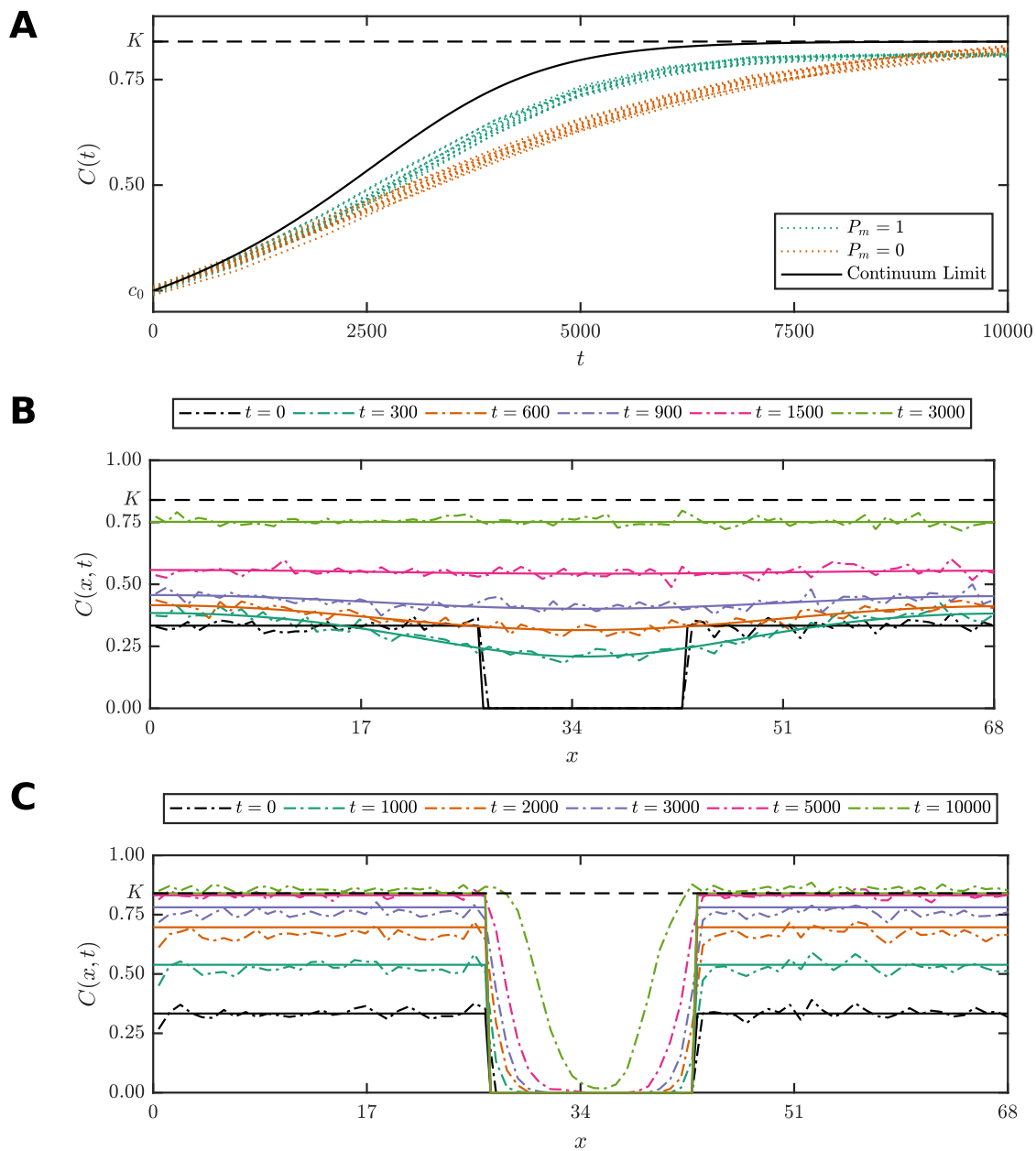


Figure F.1: Continuum-limit approximations for the (A) weak Allee model and (B)-(C) the scratch assay model plotted against stochastic simulations of the discrete model. (A) For the weak Allee model, the continuum limit (black solid) does not capture the average behavior of the discrete model for motile agents, $P_m = 1$, (green dotted) or non-motile agents, $P_m = 0$, (orange dotted). (B)-(C) For the scratch assay model, the continuum limit (solid) is a very good match of the average behavior of the (B) discrete model (dot-dashed) for motile agents, $P_m = 1$, but a very poor approximation of the average behavior of the (C) discrete model (dot-dashed) for non-motile agents, $P_m = 0$, especially in the scratch region. Parameters used in the simulations are $P_p = 1/1000$, $\lambda = P_p/\tau$, $D = P_m\delta^2/4\tau$, $K = 5/6$, and $A = 1/10$. The stochastic simulations are performed on an $I \times J$ hexagonal lattice with $I = 80$, $J = 68$, $\tau = 1$ and $\delta = 1$.

Appendix G Synthetic data

The full synthetic data used in the main manuscript for computational examples is provided in Table G.1 for the Allee effect model and in Table G.2 for the scratch assay model.

Table G.1: Synthetic data used for the weak Allee effect model example.

t	0	1,000	2,000	3,000	4,000	5,000	6,000	7,000	8,000	9,000	10,000
$\bar{C}(t)$	0.27	0.33	0.41	0.50	0.57	0.63	0.70	0.74	0.77	0.80	0.82

Table G.2: Synthetic data used for the cell culture assay model example.

$\bar{C}(x, t)$	t_0	t_1	t_2	t_3	t_4	t_5	t_6	t_7	t_8	t_9	t_{10}	
0	0.43	0.26	0.43	0.44	0.50	0.57	0.51	0.65	0.68	0.71	0.76	0.79
1	1.30	0.25	0.43	0.51	0.46	0.37	0.47	0.63	0.69	0.74	0.78	0.76
2	2.17	0.37	0.40	0.38	0.43	0.57	0.53	0.66	0.74	0.69	0.75	0.82
3	3.03	0.28	0.43	0.40	0.41	0.47	0.46	0.65	0.75	0.72	0.65	0.72
4	3.90	0.32	0.37	0.47	0.46	0.43	0.53	0.62	0.66	0.71	0.75	0.74
5	4.76	0.32	0.35	0.44	0.47	0.53	0.54	0.72	0.69	0.66	0.66	0.81
6	5.63	0.37	0.35	0.40	0.44	0.50	0.63	0.57	0.71	0.66	0.66	0.76
7	6.50	0.37	0.41	0.50	0.44	0.50	0.57	0.72	0.69	0.75	0.74	0.81
8	7.36	0.26	0.38	0.49	0.47	0.53	0.62	0.60	0.65	0.62	0.79	0.66
9	8.23	0.37	0.35	0.47	0.51	0.56	0.43	0.56	0.66	0.69	0.72	0.76
10	9.09	0.35	0.38	0.41	0.50	0.40	0.57	0.60	0.59	0.71	0.84	0.78
11	9.96	0.37	0.35	0.46	0.41	0.49	0.63	0.54	0.59	0.72	0.78	0.71
12	10.83	0.32	0.31	0.40	0.43	0.50	0.57	0.57	0.63	0.81	0.71	0.81
13	11.69	0.28	0.43	0.32	0.41	0.53	0.57	0.49	0.72	0.71	0.75	0.81
14	12.56	0.35	0.47	0.31	0.47	0.51	0.63	0.54	0.60	0.74	0.81	0.74
15	13.42	0.26	0.37	0.40	0.51	0.53	0.59	0.62	0.59	0.72	0.78	0.66
16	14.29	0.35	0.24	0.24	0.49	0.56	0.57	0.69	0.71	0.62	0.76	0.72
17	15.16	0.34	0.25	0.41	0.43	0.47	0.69	0.68	0.63	0.65	0.68	0.74
18	16.02	0.34	0.50	0.34	0.44	0.51	0.47	0.57	0.65	0.74	0.71	0.78
19	16.89	0.50	0.32	0.41	0.35	0.46	0.49	0.54	0.71	0.71	0.66	0.79
20	17.75	0.29	0.31	0.38	0.49	0.54	0.49	0.53	0.65	0.63	0.66	0.76
21	18.62	0.46	0.38	0.44	0.44	0.46	0.50	0.54	0.63	0.69	0.71	0.56
22	19.49	0.38	0.29	0.32	0.41	0.51	0.53	0.62	0.66	0.71	0.74	0.76
23	20.35	0.41	0.35	0.40	0.37	0.47	0.53	0.65	0.57	0.85	0.76	0.75
24	21.22	0.32	0.34	0.37	0.37	0.40	0.66	0.69	0.59	0.65	0.75	0.76
25	22.08	0.21	0.29	0.35	0.41	0.49	0.65	0.59	0.63	0.69	0.68	0.75
26	22.95	0.34	0.21	0.32	0.38	0.40	0.51	0.68	0.65	0.62	0.71	0.79
27	23.82	0.29	0.24	0.22	0.41	0.46	0.49	0.71	0.59	0.68	0.75	0.71
28	24.68	0.41	0.34	0.29	0.44	0.49	0.59	0.60	0.65	0.71	0.62	0.71
29	25.55	0.29	0.25	0.32	0.38	0.40	0.57	0.54	0.76	0.56	0.74	0.82
30	26.41	0.26	0.22	0.46	0.29	0.56	0.60	0.65	0.65	0.68	0.81	0.69
31	27.28	0.00	0.25	0.41	0.43	0.46	0.56	0.69	0.60	0.76	0.79	0.76
32	28.15	0.00	0.18	0.29	0.44	0.51	0.47	0.49	0.54	0.66	0.71	0.75
33	29.01	0.00	0.21	0.35	0.43	0.54	0.51	0.63	0.68	0.62	0.66	0.72
34	29.88	0.00	0.22	0.24	0.40	0.49	0.56	0.63	0.63	0.74	0.72	0.79
35	30.74	0.00	0.19	0.37	0.43	0.44	0.56	0.57	0.71	0.57	0.85	0.76
36	31.61	0.00	0.21	0.40	0.34	0.50	0.59	0.53	0.65	0.78	0.71	0.74
37	32.48	0.00	0.21	0.40	0.34	0.54	0.50	0.63	0.75	0.79	0.75	0.72
38	33.34	0.00	0.21	0.34	0.47	0.38	0.60	0.65	0.62	0.78	0.72	0.75
39	34.21	0.00	0.15	0.37	0.47	0.51	0.63	0.54	0.71	0.65	0.78	0.82
40	35.07	0.00	0.21	0.34	0.40	0.40	0.46	0.63	0.69	0.66	0.71	0.79
41	35.94	0.00	0.19	0.26	0.46	0.53	0.51	0.65	0.68	0.65	0.76	0.79
42	36.81	0.00	0.26	0.32	0.29	0.53	0.57	0.68	0.66	0.68	0.63	0.79
43	37.67	0.00	0.16	0.28	0.50	0.44	0.60	0.60	0.54	0.74	0.72	0.74
44	38.54	0.00	0.21	0.31	0.49	0.59	0.50	0.66	0.74	0.72	0.69	0.72
45	39.40	0.00	0.22	0.31	0.37	0.57	0.53	0.62	0.62	0.78	0.72	0.76
46	40.27	0.00	0.24	0.32	0.41	0.49	0.59	0.65	0.72	0.68	0.72	0.82
47	41.14	0.00	0.22	0.37	0.51	0.46	0.46	0.56	0.62	0.69	0.72	0.76
48	42.00	0.00	0.28	0.24	0.44	0.56	0.59	0.68	0.63	0.60	0.68	0.74
49	42.87	0.00	0.25	0.35	0.37	0.47	0.51	0.60	0.71	0.71	0.71	0.75
50	43.73	0.32	0.21	0.41	0.37	0.51	0.66	0.46	0.63	0.59	0.75	0.76
51	44.60	0.32	0.21	0.26	0.38	0.57	0.56	0.56	0.74	0.66	0.78	0.76
52	45.47	0.47	0.21	0.26	0.49	0.37	0.57	0.76	0.59	0.74	0.71	0.78
53	46.33	0.40	0.26	0.38	0.46	0.50	0.51	0.59	0.53	0.62	0.74	0.66
54	47.20	0.40	0.25	0.31	0.46	0.51	0.56	0.66	0.71	0.78	0.63	0.75
55	48.06	0.34	0.29	0.34	0.51	0.51	0.49	0.53	0.60	0.76	0.76	0.71
56	48.93	0.25	0.31	0.37	0.44	0.38	0.51	0.63	0.62	0.66	0.75	0.79
57	49.80	0.35	0.24	0.44	0.38	0.43	0.51	0.63	0.76	0.71	0.72	0.76
58	50.66	0.26	0.31	0.29	0.43	0.50	0.65	0.59	0.66	0.68	0.68	0.76
59	51.53	0.31	0.31	0.32	0.41	0.51	0.63	0.68	0.51	0.69	0.74	0.76
60	52.39	0.29	0.40	0.37	0.41	0.49	0.56	0.66	0.63	0.71	0.87	0.75
61	53.26	0.41	0.37	0.28	0.35	0.51	0.54	0.71	0.65	0.68	0.69	0.75
62	54.13	0.19	0.24	0.32	0.37	0.51	0.69	0.65	0.68	0.65	0.76	0.68
63	54.99	0.31	0.38	0.49	0.37	0.44	0.37	0.65	0.68	0.63	0.71	0.81
64	55.86	0.37	0.29	0.40	0.43	0.49	0.62	0.65	0.68	0.66	0.71	0.75
65	56.72	0.26	0.37	0.37	0.43	0.44	0.56	0.51	0.60	0.59	0.84	0.78
66	57.59	0.29	0.26	0.49	0.46	0.41	0.57	0.53	0.60	0.82	0.63	0.71
67	58.46	0.35	0.28	0.50	0.40	0.56	0.53	0.63	0.74	0.66	0.78	0.81
68	59.32	0.29	0.31	0.40	0.44	0.50	0.62	0.57	0.63	0.71	0.65	0.71
69	60.19	0.40	0.41	0.32	0.44	0.49	0.63	0.66	0.71	0.71	0.68	0.76
70	61.05	0.26	0.44	0.38	0.43	0.47	0.62	0.62	0.66	0.68	0.74	0.78
71	61.92	0.40	0.29	0.35	0.50	0.51	0.57	0.40	0.62	0.60	0.68	0.78
72	62.79	0.26	0.41	0.41	0.34	0.47	0.66	0.60	0.60	0.72	0.76	0.72
73	63.65	0.40	0.50	0.38	0.43	0.56	0.59	0.53	0.69	0.76	0.74	0.72
74	64.52	0.35	0.29	0.43	0.62	0.43	0.53	0.59	0.66	0.63	0.76	0.68
75	65.38	0.34	0.43	0.47	0.47	0.51	0.65	0.54	0.62	0.72	0.76	0.69
76	66.25	0.28	0.47	0.40	0.53	0.53	0.54	0.72	0.65	0.68	0.68	0.74
77	67.12	0.35	0.37	0.37	0.56	0.54	0.49	0.62	0.74	0.75	0.78	0.82
78	67.98	0.37	0.47	0.38	0.41	0.63	0.62	0.59	0.59	0.81	0.76	0.75
79	68.85	0.28	0.35	0.40	0.37	0.51	0.50	0.71	0.71	0.72	0.66	0.74

References

- [1] D. J. G. Agnew, J. E. F. Green, T. M. Brown, M. J. Simpson, and B. J. Binder. Distinguishing between mechanisms of cell aggregation using pair-correlation functions. *Journal of Theoretical Biology*, 352:16–23, 2014. DOI:10.1016/j.jtbi.2014.02.033
- [2] R. E. Baker, J.-M. Peña, J. Jayamohan, and A. Jérusalem. Mechanistic models versus machine learning, a fight worth fighting for the biological community? *Biology Letters*, 14:20170660, 2018. DOI:10.1098/rsbl.2017.0660
- [3] M. Banterle, C. Grazian, A. Lee, and C. P. Robert. Accelerating Metropolis-Hastings algorithms by delayed acceptance. *Foundations of Data Science*, 1:103–128, 2019. DOI:10.3934/fods.2019005
- [4] C. P. Barnes, S. Filippi, M. P. H. Stumpf, and T. Thorne. Considerate approaches to constructing summary statistics for ABC model selection. *Statistics and Computing*, 22:1181–1197, 2012. DOI:10.1007/s11222-012-9335-7
- [5] M. A. Beaumont, W. Zhang, and D. J. Balding. Approximate Bayesian computation in population genetics. *Genetics*, 162:2025–2035, 2002.
- [6] M. A. Beaumont, J.-M. Cornuet, J.-M. Marin, and C. P. Robert. Adaptive approximate Bayesian computation. *Biometrika*, 96:983–990, 2009. DOI:10.1093/biomet/asp052
- [7] R. N. Binny, P. Haridas, A. James, R. Law, M. J. Simpson, and M. J. Plank. Spatial structure arising from neighbour-dependent bias in collective cell movement. *PeerJ*, 4:e1689, 2016. DOI:10.7717/peerj.1689
- [8] A. J. Black, and A. J. McKane. Stochastic formulation of ecological models and their applications. *Trends in Ecology & Evolution*, 27:337–345, 2012. DOI:10.1016/j.tree.2012.01.014
- [9] A. P. Browning, P. Haridas, and M. J. Simpson. A Bayesian sequential learning framework to parameterise continuum models of melanoma invasion into human skin. *Bulletin of Mathematical Biology*, 81:676–698, 2019. DOI:10.1007/s11538-018-0532-1
- [10] A. P. Browning, S. W. McCue, R. N. Binny, M. J. Plank, E. T. Shah, and M. J. Simpson. Inferring parameters for a lattice-free model of cell migration and proliferation using experimental data. *Journal of Theoretical Biology*, 437:251–260, 2018. DOI:10.1016/j.jtbi.2017.10.032
- [11] A. P. Browning, S. W. McCue, and M. J. Simpson. A Bayesian computational approach to explore the optimal duration of a cell proliferation assay. *Bulletin of Mathematical Biology*, 79:1888–1906, 2017. DOI:10.1007/s11538-017-0311-4
- [12] K. Böttger, H. Hatzikirou, A. Voss-Böhme, E. A. Cavalcanti-Adam, M. A. Herrero, and A. Deutsch. An emerging Allee effect is critical for tumor initiation and persistence. *PLOS Computational Biology*, 11:e1004366, 2015. DOI:10.1371/journal.pcbi.1004366

- [13] E. O. Buzbas, and N. A. Rosenberg. AABC: Approximate approximate Bayesian computation for inference in population-genetic models. *Theoretical Population Biology*, 99:31–42, 2015. DOI:10.1016/j.tpb.2014.09.002
- [14] T. Callaghan, E. Khain, L. M. Sander, and R. M. Ziff. A stochastic model for wound healing. *Journal of Statistical Physics*, 122:909–924, 2006. DOI:10.1007/s10955-006-9022-1
- [15] Z. Cao, and R. Grima. Linear mapping approximations of gene regulatory networks with stochastic dynamics. *Nature Communications*, 9:3305, 2018. DOI:10.1038/s41467-018-05822-0
- [16] C. L. P. Chen, and C.-Y. Zhang. Data-intensive applications, challenges, techniques and technologies: a survey on big data. *Information Sciences*, 275:314–347, 2014. DOI:10.1016/j.ins.2014.01.015
- [17] O. A. Chkrebtii, E. K. Cameron, D. A. Campbell, and E. M. Bayne. Transdimensional approximate Bayesian computation for inference on invasive species models with latent variables of unknown dimension. *Computational Statistics and Data Analysis*, 86:97–110, 2015. DOI:10.1016/j.csda.2015.01.002
- [18] E. A. Codling, M. J. Plank, and S. Benhamou. Random walk models in biology. *Journal of The Royal Society Interface*, 5:813–834, 2008. DOI:10.1098/rsif.2008.0014
- [19] S. L. Cotter, M. Dashti, and A. M. Stuart. Approximation of Bayesian inverse problems for PDEs. *SIAM Journal on Numerical Analysis*, 48:322–345, 2010. DOI:10.1137/090770734
- [20] P. V. Coveney, E. R. Dougherty, and R. R. Highfield. Big data need big theory too. *Philosophical Transactions of the Royal Society A: Mathematical, Physical and Engineering Sciences*, 374:20160153, 2016. DOI:10.1098/rsta.2016.0153
- [21] D. L. DeAngelis and V. Grimm. Individual-based models in ecology after four decades. *F1000Prime Reports*, 6:39, 2014. DOI:10.12703/P6-39
- [22] P. Del Moral, A. Doucet, and A. Jasra. Sequential Monte Carlo samplers. *Journal of the Royal Statistical Society: Series B (Statistical Methodology)*, 68:411–436, 2006. DOI:10.1111/j.1467-9868.2006.00553.x
- [23] B. Drawert, M. Griesemer, L. R. Petzold, and C. J. Briggs. Using stochastic epidemiological models to evaluate conservation strategies for endangered amphibians. *Journal of the Royal Society Interface*, 14:20170480, 2017. DOI:10.1098/rsif.2017.0480
- [24] C. C. Drovandi and A. N. Pettitt. Estimation of parameters for macroparasite population evolution using approximate Bayesian computation. *Biometrics*, 67:225–233, 2011. DOI:10.1111/j.1541-0420.2010.01410.x
- [25] L. Edelstein-Keshet. *Mathematical Models in Biology*. Society for Industrial and Applied Mathematics, 2005.
- [26] A. M. Ellison. Bayesian inference in ecology. *Ecology Letters*, 7:509–520, 2004. DOI:10.1111/j.1461-0248.2004.00603.x

- [27] R. G. Everitt and P. A. Rowińska. Delayed acceptance ABC-SMC. *ArXiv e-prints*, 2017. arXiv:1708.02230 [stat.CO]
- [28] P. Fearnhead and D. Prangle. Constructing summary statistics for approximate Bayesian computation: semi-automatic approximate Bayesian computation. *Journal of the Royal Statistical Society Series B (Statistical Methodology)*, 74:419–474, 2012. DOI:10.1111/j.1467-9868.2011.01010.x
- [29] E. Fehlberg. Low-order classical Runge-Kutta formulas with step size control and their application to some heat transfer problems. *NASA Technical Report*, R-315, 1969.
- [30] S. Filippi, C. P. Barnes, J. Cornebise, and M. P. H. Stumpf. On optimality of kernels for approximate Bayesian computation using sequential Monte Carlo. *Statistical Applications in Genetics and Molecular Biology*, 12:87–107, 2013. DOI:10.1515/sagmb-2012-0069
- [31] A. Gelman, J. B. Carlin, H. S. Stern, D. B. Dunson, A. Vehtari, and D. B. Rubin. *Bayesian Data Analysis*. Chapman & Hall/CRC, 3rd edition, 2014.
- [32] M. B. Giles. Multilevel Monte Carlo methods. *Acta Numerica*, 24:259–328, 2015. DOI:10.1017/S096249291500001X
- [33] A. Golightly, D. A. Henderson, and C. Sherlock. Delayed acceptance particle MCMC for exact inference in stochastic kinetic models. *Statistics and Computing*, 25:1039–1055, 2015. DOI:10.1007/s11222-014-9469-x
- [34] R. Gunawan, Y. Cao, L. Petzold, and F. J. Doyle III. Sensitivity analysis of discrete stochastic systems. *Biophysical Journal*, 88:2530–2540, 2005. DOI:10.1529/biophysj.104.053405
- [35] D. J. Higham. Modeling and simulating chemical reactions. *SIAM review*, 50:347–368, 2008. DOI:10.1137/060666457
- [36] P. B. Holden, N. R. Edwards, A. Ridgwell, R. D. Wilkinson, K. Fraedrich, F. Lunkeit, H. Pollit, J. F. Mercure, P. Salas, A. Lam, F. Knobloch, U. Chewpreecha, and J. E. Viñuales. Climate–carbon cycle uncertainties and the Paris Agreement. *Nature Climate Change*, 8:609–613, 2018. DOI:10.1038/s41558-018-0197-7
- [37] A. Iserles. *A First Course in the Numerical Analysis of Differential Equations*. Cambridge University Press, 2nd Edition, 2008.
- [38] A. Jasra, S. Jo, D. Nott, C. Shoemaker, and R. Tempone. Multilevel Monte Carlo in approximate Bayesian computation. *Stochastic Analysis and Applications*, 37:346–360, 2019. DOI:10.1080/07362994.2019.1566006
- [39] W. Jin, C. J. Penington, S. W. McCue, and M. J. Simpson. Stochastic simulation tools and continuum models for describing two-dimensional collective cell spreading with universal growth functions. *Physical Biology*, 13:056003, 2016. DOI:10.1088/1478-3975/13/5/056003

- [40] W. Jin, E. T. Shah, C. J. Penington, S. W. McCue, P. K. Maini, and M. J. Simpson. Logistic proliferation of cells in scratch assays is delayed. *Bulletin of Mathematical Biology*, 79:1028–1050, 2017. DOI:10.1007/s11538-017-0267-4
- [41] S. T. Johnston, M. J. Simpson, and M. J. Plank. Lattice-free descriptions of collective motion with crowding and adhesion. *Physical Review E*, 88:062720, 2013. DOI:10.1103/PhysRevE.88.062720
- [42] S. T. Johnston, M. J. Simpson, D. L. S. McElwain, B. J. Binder, and J. V. Ross. Interpreting scratch assays using pair density dynamics and approximate Bayesian computation. *Open Biology*, 4, 2014. DOI:10.1098/rsob.140097
- [43] T. E. King, G. G. Fortes, P. Balaesque, M. G. Thomas, D. Balding, P. M. Delsler, R. Neumann, W. Parson, M. Knapp, S. Walsh, L. Tonasso, J. Holt, M. Kayser, J. Appleby, P. Forster, D. Ekserdjian, M. Hofreiter, and K. Schürer. Identification of the remains of King Richard III. *Nature Communications*, 5:5631, 2014. DOI:10.1038/ncomms6631
- [44] S. Kullback and R. A. Leibler. On information and sufficiency. *The Annals of Mathematical Statistics*, 22:79-86, 1951. DOI:10.1214/aoms/1177729694
- [45] R. Law, D. J. Murrell, and U. Dieckmann. Population growth in space and time: spatial logistic equations. *Ecology*, 84:252–262, 2003. DOI:10.1890/0012-9658(2003)084[0252:PGISAT]2.0.CO;2
- [46] B. A. J. Lawson, C. C. Drovandi, N. Cusimano, P. Burrage, B. Rodriguez, and K. Burrage. Unlocking data sets by calibrating populations of models to data density: A study in atrial electrophysiology. *Science Advances*, 4:e1701676, 2018. DOI:10.1126/sciadv.1701676
- [47] J. Lei and P. Bickel. A moment matching ensemble filter for nonlinear non-Gaussian data assimilation. *Monthly Weather Review*, 139:3964–3973, 2011. DOI:10.1175/2011MWR3553.1
- [48] C. Lester. Multi-level approximate Bayesian computation. *ArXiv e-prints*, 2018. arXiv:1811.08866 [q-bio.QM]
- [49] C. Lester, C. A. Yates, and R. E. Baker. Efficient parameter sensitivity computation for spatially extended reaction networks. *The Journal of Chemical Physics*, 146:044106, 2017. DOI:10.1063/1.4973219
- [50] C.-C. Liang, A. Park, and J.-L. Guan. In vitro scratch assay: a convenient and inexpensive method for analysis of cell migration in vitro. *Nature Protocols*, 2:329–333, 2007. DOI:10.1038/nprot.2007.30
- [51] S. Liao, T. Vejchodský, and R. Erban. Tensor methods for parameter estimation and bifurcation analysis of stochastic reaction networks. *Journal of the Royal Society Interface*, 12:20150233, 2015. DOI:10.1098/rsif.2015.0233
- [52] G. Lillacci, and M. Khammash. Parameter estimation and model selection in computational biology. *PLOS Computational Biology*, 6:e1000696, 2010. DOI:10.1371/journal.pcbi.1000696

- [53] Q.-H. Liu, M. Ajelli, A. Aleta, S. Merler, Y. Moreno, and A. Vespignani. Measurability of the epidemic reproduction number in data-driven contact networks. *The Proceedings of the National Academy of Sciences of the United States of America*, 115:12680–12685, 2018. DOI:10.1073/pnas.1811115115
- [54] A.-S. Malaspinas, M. C. Westaway, C. Muller, V. C. Sousa, O. Lao, I. Alves, A. Bergström, G. Athanasiadis, J. Y. Cheng, J. E. Crawford, et al. A genomic history of Aboriginal Australia. *Nature*, 538:207–214, 2016. DOI:10.1038/nature18299
- [55] S. Marino, I. B. Hogue, C. J. Ray, and D. E Kirschner. A methodology for performing global uncertainty and sensitivity analysis in systems biology. *Journal of Theoretical Biology*, 254:178–196, 2008. DOI:10.1016/j.jtbi.2008.04.011
- [56] P. Marjoram, J. Molitor, V. Plagnol, and S. Tavaré. Markov chain Monte Carlo without likelihoods. *Proceedings of the National Academy of Sciences of the United States of America*, 100:15324–15328, 2003. DOI:10.1073/pnas.0306899100
- [57] A. J. McLane, C. Semeniuk, G. J. McDermid, and D. J. Marceau. The role of agent-based models in wildlife ecology and management. *Ecology Modelling*, 222:1544–1556, 2011. DOI:10.1016/j.ecolmodel.2011.01.020
- [58] J. D. Murray. *Mathematical Biology: I. An Introduction*. Springer, New York, 2002.
- [59] A. O’Dea, H. A. Lessios, A. G. Coates, R. I. Eytan, S. A. Restrepo-Moreno, A. L. Cione, L. S. Collins, A. de Queiroz, D. W. Farris, R. D. Norris, et al. Formation of the Isthmus of Panama. *Science Advances*, 2:e1600883, 2016. DOI:10.1126/sciadv.1600883
- [60] D. Prangle. Lazy ABC. *Statistics and Computing*, 26:171–186, 2016. DOI:10.1007/s11222-014-9544-3
- [61] T. P. Prescott and R. E. Baker. Multifidelity approximate Bayesian computation. *ArXiv e-prints*, 2018. arXiv:1811.09550 [stat.CO]
- [62] W. H. Press, S. A. Teukolsky, W. T. Vetterling, and B. P. Flannery. *Numerical Recipes in C: The Art of Scientific Computing*. Cambridge University Press, 1997.
- [63] J K Pritchard, M T Seielstad, A Perez-Lezaun, and M W Feldman. Population growth of human y chromosomes: a study of y chromosome microsatellites. *Molecular Biology and Evolution*, 16:1791–1798, 1999. DOI:10.1093/oxfordjournals.molbev.a026091
- [64] J. A. J. Rynn, S. L. Cotter, C. E. Powell, and L. Wright. Surrogate accelerated Bayesian inversion for the determination of the thermal diffusivity of a material. *Metrologia*, 59:015018, 2019. DOI:10.1088/1681-7575/aaf984
- [65] M. J. Simpson, B. J. Binder, P. Haridas, B. K. Wood, K. K. Treloar, D. L. S. McElwain, and R. E. Baker. Experimental and modelling investigation of monolayer development with clustering. *Bulletin of Mathematical Biology*, 75:871–889, 2013. DOI:10.1007/s11538-013-9839-0

- [66] M. J. Simpson, K. A. Landman, and K. Bhaganagarapu. Coalescence of interacting cell populations. *Journal of Theoretical Biology*, 247:525–543, 2007. DOI:10.1016/j.jtbi.2007.02.020
- [67] M. J. Simpson, K. A. Landman, and B. D. Hughes. Cell invasion with proliferation mechanisms motivated by time-lapse data. *Physica A: Statistical Mechanics and its Applications*, 389:3779–3790, 2010. DOI:10.1016/j.physa.2010.05.020
- [68] S. A. Sisson, Y. Fan, and M. M. Tanaka. Sequential Monte Carlo without likelihoods. *Proceedings of the National Academy of Sciences of the United States of America*, 104:1760–1765, 2007. DOI:10.1073/pnas.0607208104
- [69] S. A. Sisson, Y. Fan, and M. Beaumont. *Handbook of Approximate Bayesian Computation*. Chapman & Hall/CRC, 1st edition, 2018.
- [70] S. W. Sloan and A. J. Abbo. Biot consolidation analysis with automatic time stepping and error control Part 1: theory and implementation. *International Journal for Numerical and Analytical Methods in Geomechanics*, 23:467–492, 1999. DOI:10.1002/(SICI)1096-9853(199905)23:6<467::AID-NAG949>3.0.CO;2-R
- [71] M. P. H. Stumpf. Approximate Bayesian inference for complex ecosystems. *F1000Prime Reports*, 6:60, 2014. DOI:10.12703/P6-60
- [72] B. Sun, J. Fen, and K. Saenko. Return of frustratingly easy domain adaptation. *Proceedings of the Thirtieth AAAI Conference on Artificial Intelligence*, AAAI Press, 2058–2065, 2016.
- [73] S. Tavaré, D. J. Balding, R. C. Griffiths, and P. Donnelly. Inferring coalescence times from DNA sequence data. *Genetics*, 145:505–518, 1997.
- [74] C. M. Taylor and A. Hastings. Allee effects in biological invasions. *Ecology Letters*, 8:895–908, 2005. DOI:10.1111/j.1461-0248.2005.00787.x
- [75] The Event Horizon Telescope Collaboration, K. Akiyama, A. Alberdi, W. Alef, K. Asada, R. Azulay, A.-K. Bacsko, D. Ball, M. Baloković, J. Barrett, et al. First M87 Event Horizon Telescope results. VI. The shadow and mass of the central black hole. *The Astrophysical Journal Letters*, 875:L6, 2019. DOI:10.3847/2041-8213/ab1141
- [76] T. Toni, D. Welch, N. Strelkowa, A. Ipsen, and M. P. H. Stumpf. Approximate Bayesian computation scheme for parameter inference and model selection in dynamical systems. *Journal of the Royal Society Interface*, 6:187–202, 2008. DOI:10.1098/rsif.2008.0172
- [77] A. Tsoularis and J. Wallace. Analysis of logistic growth models. *Mathematical Biosciences*, 179:21–55, 2002. DOI:10.1016/S0025-5564(02)00096-2
- [78] C. E. Vincenot, F. Carteni, S. Mazzoleni, M. Rietkerk, and F. Giannino. Spatial self-organization of vegetation subject to climatic stress—insights from a system dynamics—individual-based hybrid model. *Frontiers in Plant Science*, 7:636, 2016. DOI:10.3389/fpls.2016.0063

- [79] B. N. Vo, C. C. Drovandi, A. N. Pettit, and G. J. Pettet. Melanoma cell colony expansion parameters revealed by approximate Bayesian computation. *PLoS Computational Biology*, 11:e1004635, 2015. DOI:10.1371/journal.pcbi.1004635
- [80] B. N. Vo, C. C. Drovandi, A. N. Pettit, and M. J. Simpson. Quantifying uncertainty in parameter estimates for stochastic models of collective cell spreading using approximate Bayesian computation. *Mathematical Biosciences*, 263:133–142, 2015. DOI:10.1016/j.mbs.2015.02.010
- [81] J. von Hardenberg, E. Meron, M. Shachak, and Y. Zarmi. Diversity of vegetation patterns and desertification. *Physical Review Letters*, 87:198101, 2001. DOI:10.1103/PhysRevLett.87.198101
- [82] Y. Wang, J. Shi, and J. J. Wang. Persistence and extinction of population in reaction–diffusion–advection model with strong Allee effect growth. *Journal of Mathematical Biology*, 78:2093–2140, 2019. DOI:10.1007/s00285-019-01334-7
- [83] D. J. Warne, R. E. Baker, and M. J. Simpson. Optimal quantification of contact inhibition in cell populations. *Biophysical Journal*, 113:1920–1924, 2017. DOI:10.1016/j.bpj.2017.09.016
- [84] D. J. Warne, R. E. Baker, and M. J. Simpson. Multilevel rejection sampling for approximate Bayesian computation. *Computational Statistics and Data Analysis*, 124:71–86, 2018. DOI:10.1016/j.csda.2018.02.009
- [85] D. J. Warne, R. E. Baker, and M. J. Simpson. Using experimental data and information criteria to guide model selection for reaction–diffusion problems in mathematical biology. *Bulletin of Mathematical Biology*, 81(6):1760–1804, 2019. DOI:10.1007/s11538-019-00589-x
- [86] D. J. Warne, R. E. Baker, and M. J. Simpson. Simulation and inference algorithms for stochastic biochemical reaction networks: from basic concepts to state-of-the-art. *Journal of the Royal Society Interface*, 16:20180943, 2019. DOI:10.1098/rsif.2018.0943
- [87] D. J. Wilkinson. Stochastic modelling for quantitative description of heterogeneous biological systems. *Nature Review Genetics*, 10:122–133, 2009. DOI:10.1038/nrg2509
- [88] T. P. Witelski. Merging traveling waves for the porous-Fisher’s equation. *Applied Mathematics Letters*, 8:57–62, 1995. DOI:10.1016/0893-9659(95)00047-T
- [89] M. L. Woods and C. P. Barnes. Mechanistic modelling and Bayesian inference elucidates the variable dynamics of double-strand break repair. *PLoS Computational Biology*, 12(10):e1005131, 2016. DOI:10.1371/journal.pcbi.1005131
- [90] C. Zechner, J. Ruess, P. Krenn, S. Pelet, M. Peter, J. Lygeros, and H. Koeppl. Moment-based inference predicts bimodality in transient gene expression. *Proceedings of the National Academy of Sciences of the United States of America*, 109:8340–8345, 2012. DOI:10.1073/pnas.1200161109